HHS Public Access

Author manuscript

Cell Rep. Author manuscript; available in PMC 2022 August 29.

Published in final edited form as:

Cell Rep. 2022 August 23; 40(8): 111250. doi:10.1016/j.celrep.2022.111250.

Partitioned usage of chromatin remodelers by nucleosome-displacing factors

Hengye Chen[1,2], **Hungyo Kharerin**[1,2], **Archana Dhasarathy**[3], **Michael Kladde**[4,5], **Lu Bai**[1,2,6,7,*]

[1]Department of Biochemistry and Molecular Biology, The Pennsylvania State University, University Park, PA 16802, USA

[2]Center for Eukaryotic Gene Regulation, The Pennsylvania State University, University Park, PA 16802, USA

[3]Department of Biomedical Sciences, University of North Dakota School of Medicine and Health Sciences, Grand Forks, ND 58201, USA

[4]Department of Biochemistry and Molecular Biology, College of Medicine, University of Florida, Gainesville, FL 32610, USA

[5]UF Health Cancer Center, University of Florida, Gainesville, FL 32610, USA

[6]Department of Physics, The Pennsylvania State University, University Park, PA 16802, USA

[7]Lead contact

SUMMARY

Nucleosome-displacing-factors (NDFs) in yeast, similar to pioneer factors in higher eukaryotes, can open closed chromatin and generate nucleosome-depleted regions (NDRs). NDRs in yeast are also affected by ATP-dependent chromatin remodelers (CRs). However, how NDFs and CRs coordinate in nucleosome invasion and NDR formation is still unclear. Here, we design a high-throughput method to systematically study the interplay between NDFs and CRs. By combining an integrated synthetic oligonucleotide library with DNA methyltransferase-based, single-molecule nucleosome mapping, we measure the impact of CRs on NDRs generated by individual NDFs. We find that CRs are dispensable for nucleosome invasion by NDFs, and they function downstream of NDF binding to modulate the NDR length. A few CRs show high specificity toward certain NDFs; however, in most cases, CRs are recruited in a factor-nonspecific

*Correspondence: lub15@psu.edu.

AUTHOR CONTRIBUTIONS

L.B. and H.C. designed the experiments; H.C. performed most of the experiments and data analysis; H.K. and L.B. carried out the genome-wide data analysis; A.D. and M.K. constructed the DNA methyltransferase expression systems; H.C. and L.B. wrote the manuscript.

SUPPLEMENTAL INFORMATION

Supplemental information can be found online at https://doi.org/10.1016/j.celrep.2022.111250.

DECLARATION OF INTERESTS

The authors declare no competing interests.

and NDR length-dependent manner. Overall, our study provides a framework to investigate how NDFs and CRs cooperate to regulate chromatin opening.

Graphical abstract

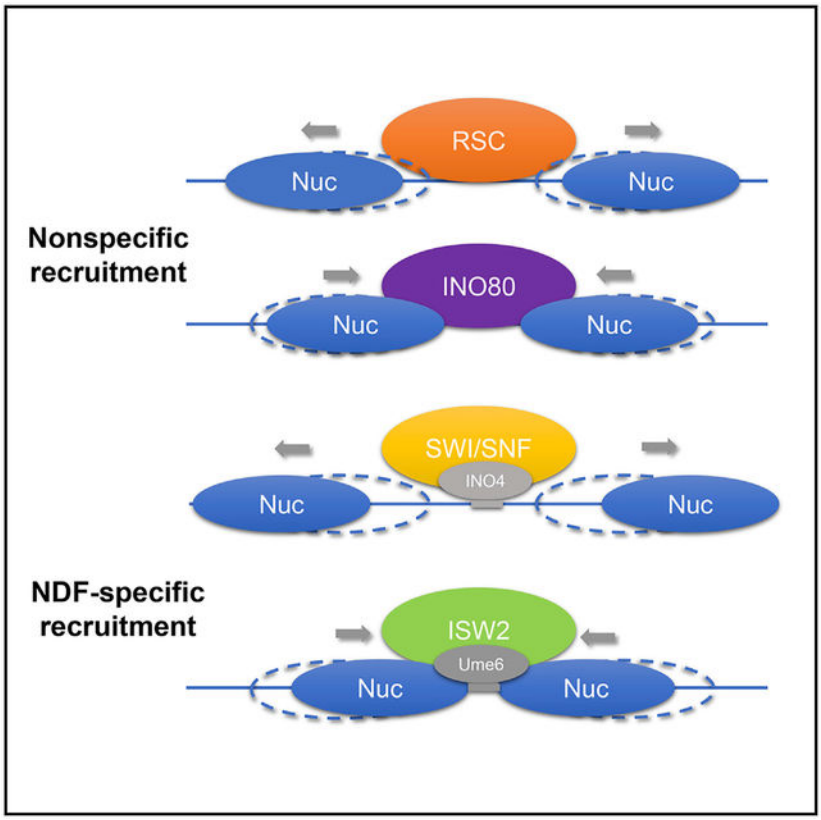

In brief

Chromatin accessibility in yeast is regulated by nucleosome-displacing-factors (NDFs) and chromatin remodelers (CRs). Chen et al. show that NDFs first invade into nucleosomes and then recruit CRs to modulate the NDR length. NDF-specific and NDR length-dependent recruitment of CRs allow partitioned usage of CRs by NDFs.

INTRODUCTION

In eukaryotic cells, genomic DNA is compacted into chromatin. The basic unit of chromatin is the nucleosome, composed of DNA wrapped around a core histone octamer. The extensive interactions between histones and DNA in the nucleosome present a formidable barrier to binding for most transcription factors (TFs). However, a small fraction of TFs can access nucleosomal DNA and generate nucleosome-depleted regions (NDRs) (Bai et al., 2011; Hartley and Madhani, 2009; Struhl and Segal, 2013; van Bakel et al., 2013; Yan et al., 2018). This subset of TFs, named nucleosome-displacing factors (NDFs) in yeast (Yan et al., 2018) and pioneer factors (PFs) (Zaret and Carroll, 2011) in higher eukaryotes, facilitates the binding of other TFs and allows them to regulate transcription. As upstream

factors in the transcription pathway, NDFs and PFs play essential roles in gene regulation. During development, PFs function as “master regulators” to direct cell fate and cellular reprogramming (Drouin, 2014; Iwafuchi-Doi and Zaret, 2014). Mis-regulation of PFs is linked to cancer and developmental diseases (Jeong et al., 2014; Mueller et al., 2003; Wang et al., 2007).

Despite recent progress in characterization of the functions of NDFs and PFs, the detailed molecular pathway of nucleosome invasion and NDR formation remains unclear. Purified NDFs or PFs can associate with binding sites near the edges of nucleosomes *in vitro*, but such binding is usually achieved by DNA unwrapping without histone movement or eviction (Donovan et al., 2019; Garcia et al., 2019). The *in vitro* binding affinities of these factors tend to decrease when their motifs are closer to the nucleosome pseudodyad, but at least some NDFs can efficiently invade nucleosomes through these embedded sites to generate NDRs *in vivo* (Yan et al., 2018). These observations raise the possibility that additional factors may be required to facilitate nucleosome invasion and displacement by NDFs/PFs *in vivo*. In addition, while all NDFs can reduce local nucleosome occupancy near their consensus motifs, they lead to different configurations of nucleosome positioning, even in the same sequence context. For example, Reb1 generates a broad NDR that is ~200 base pairs (bp) in size, whereas Ume6 gives rise to a narrow NDR that is similar to canonical linker DNA (Yan et al., 2018). The mechanism(s) underlying such length variation is not well understood.

The questions above prompted us to investigate the coordination between NDFs and chromatin remodelers (CRs). CRs use energy derived from ATP hydrolysis to slide and evict nucleosomes, and therefore, may facilitate NDF invasion by enhancing nucleosome mobility. Such CR function *upstream* of NDF binding was implicated in some cases, e.g., BRG1, an ATPase subunit within the SWI/SNF family, was shown to promote the binding of PFs such as OCT4, SOX2, and NANOG (King and Klose, 2017). Another non-mutually exclusive possibility is that CRs are recruited *downstream* of NDF binding to reposition the nearby nucleosomes. Different families of CRs can move nucleosomes in different directions, and mutations of different CRs lead to distinct changes in nucleosome positioning (Hartley and Madhani, 2009; Kelso et al., 2017; Krietenstein et al., 2016; Kubik et al., 2019; Schick et al., 2019; Yen et al., 2012). Therefore, it is possible that the specificity of different NDFs toward CRs contributes to the variations in NDR length. To test these hypotheses, it is necessary to compare CR impacts on the nucleosome displacement activities of individual NDFs systematically.

Previous *in vivo* studies of CRs and nucleosome positioning usually survey the native genome. Although CR mutations have been shown to affect NDRs, these data are confounded by two issues. First, native NDRs tend to be associated with multiple NDFs and other TFs that have no nucleosome-displacing activity (Bai et al., 2011), all of which can potentially recruit CRs. These CRs may work independently, cooperatively, or antagonistically, making the effect difficult to interpret. Second, nucleosome positioning is influenced by the intrinsic affinities of histones for specific DNA sequences (Struhl and Segal, 2013), and CR effect on NDR sizes may depend on the sequence context. In this work, we avoided these problems by using an Integrated Synthetic Oligo (ISO) assay,

where we engineered well-defined NDF motifs into the same background sequence so that individual NDFs can be studied in an identical chromatin context. We used a DNA methyltransferase-based method to map nucleosome positioning at the single-cell level, which allows us to separately measure NDR proportion (fraction of cells that contain NDR) and length (average NDR size in the subset of cells that contain NDR). We found that CR depletions tend to have a larger effect on NDR length than on NDR proportion. In one instance, CR depletion did not affect the rate of NDF binding and nucleosome displacement. These results suggest that CRs function downstream of NDFs, i.e., NDFs bind to DNA first and recruit CRs to reshape NDRs. The CR effect shows both factor specificity and NDR length dependence. In particular, Ino4, Stb5, and Tea1 recruit SWI/SNF to generate extra-long NDRs, and Ume6 and Rfx1 recruit ISW2 to form extra-short NDRs. RSC, INO80, and ISW2 (in the absence of Ume6 or Rfx1) modulate NDRs in a largely factor-nonspecific but length-dependent manner. Overall, our study represents a framework to investigate the coordination between NDFs and CRs on NDR generation systematically.

RESULTS

DNA methyltransferase-based method to study nucleosome positioning on an ISO library

To investigate how NDFs and CRs cooperate to regulate NDRs, we developed a high-throughput method to study nucleosome positioning near different NDF motifs engineered into the same sequence context (STAR Methods). In a previous study, we screened 104 sequence-specific TFs in budding yeast and identified 29 NDFs with nucleosome-displacing activities (Yan et al., 2018). These NDFs include six that have strong nucleosome displacement activity and can reduce local nucleosome occupancy with a single motif (group 1) and 23 weak ones that require multiple motifs to displace nucleosomes (group 2). To study all of these NDFs in parallel, we designed 169 synthetic oligos, each containing one group 1 motif or two to three group 2 motifs at variable locations within nucleosome −4 (Figure 1A and Table S1). This library also included three oligos with *tetO*, the recognition motif of the bacterial repressor TetR (single motif at −13 or −43, as well as double motif at −13 and −43). When TetR is highly expressed in yeast, it leads to NDR formation over *tetO* (Yan et al., 2018). These mixed oligos were inserted into a well-positioned nucleosome array in the *HO* promoter background and integrated into the *CLN2* locus in a yeast strain that expresses exogenous TetR (Figure 1A). We then probed the NDR configurations in this ISO library in the presence or absence of CRs. Since TetR is unlikely to have specific interactions with CRs, it is used as a negative control to compare with endogenous NDFs.

To map nucleosome positioning over the highly similar ISO sequences in parallel, the commonly used micrococcal-nuclease (MNase) assay is unsuitable. This is because the linkage between neighboring nucleosomes and the NDF motif would be lost after MNase digestion, and such linkage is essential to differentiate nucleosome positioning generated by different NDFs. We therefore used a DNA methyltransferase-based approach for nucleosome mapping (Jessen et al., 2004, 2006). Briefly, we induced the expression of a GC methyltransferase, M.CviPI (Xu et al., 1998), which selectively methylates the cytosine in GC dinucleotide within accessible chromatin regions (Figure 1B). The methylation status was then measured by bisulfite conversion of the genomic DNA, followed by

PCR amplification of a 1,278-bp region over the synthetic *HO* promoter variants, and sequencing the amplicon using the high-fidelity, circular consensus Pacific Biosciences (PacBio) platform. Long PacBio sequencing reads allow multiple nucleosomes to be mapped on a continuous stretch of DNA. Library sequences can be differentiated based on the NDF motifs as part of the sequencing reads. Furthermore, each sequencing read reflects the nucleosome positioning in a *single cell*, allowing us to extract NDR length and proportion separately (STAR Methods).

To probe the function of CRs, we mapped the nucleosomes in strains where a single CR was anchored away (STAR Methods). In previous genome-wide studies, mutations of RSC, ISW2, SWI/SNF, and INO80 were found to affect NDR sizes (Kubik et al., 2019; Yen et al., 2012). We therefore selected these four CRs in this study. The changes in methylation pattern upon CR depletion were used to determine the role of the CR in NDR formation (Figure 1B). Our ability to probe NDR length and proportion is critical for differentiating CR activities upstream and downstream of NDF binding: upstream activity would lead to enhanced NDF binding and NDR proportion, and downstream activity would result in altered NDR length. Comparison among NDRs generated by different NDFs (including TetR) in the same sequence context allows us to identify factor specificity and length dependence of CR function.

NDFs generate variable nucleosome positioning patterns in wild-type cells

We first analyzed nucleosome positioning over the synthetic oligos and the nearby regions in the wild-type (WT) strain. The methylation heatmap over the background sequence (*HO* promoter with no NDF motif) is shown in the left panel of Figure 1C, where the red color represents unprotected regions that are methylated. Nucleosome positions were predicted based on the methylation pattern in each single read (“Methyl model”) (Figure 1C right panel, Figures S1A–S1D), which agrees well with the MNase measurements (Figure 1D). As expected, most GCs in background reads are hypomethylated, corresponding to a tightly packed nucleosome array (nucleosomes −6 to −1). However, there are heterogeneous methylation signals, indicating that DNA can be exposed stochastically over this region. Note that in Figure 1C, nucleosome −4 appears to be the least stable because we sorted the reads by the nucleosome −4 occupancy. When sorted by other nucleosomes, similar openings can be seen in each case (Figure S1E). An engineered Abf1 motif inside nucleosome −4 drastically enhanced the methylation level in the motif-proximal regions, while a mutated Abf1 motif (Abf1m) at the same location had little effect on nucleosome positioning (Figures 1E and 1F). These data clearly demonstrate the nucleosome displacement activity of Abf1.

From the methylation and modeled nucleosome occupancy, we calculated the NDR proportion (fraction of reads where we can detect NDR) and NDR length (averaged length of NDRs within the NDR + subpopulation) (Figures S1C and S1D, and Table S2). These values derived from two biological replicates are highly reproducible (Figure S1F). The radar plots in Figure 1G show the NDR length and proportion measured in the full ISO library. Importantly, different NDFs with the same location and copy number of motifs generate different NDR patterns in the same sequence context. For example, Reb1 at −40

generates longer NDRs than Cbf1 at the same location, and three Ino4 motifs generate a much longer NDR than three Ume6 motifs. These results are confirmed with MNase assay (Figure S1G). NDR lengths over different ISO sequences fall into a Gaussian distribution with outliers on either side (extra-short and extra-long NDRs) (Figure S1H). These data indicate that NDFs have intrinsically different activities in nucleosome repositioning.

NDR length and proportion on different sequences show modest positive correlation (Figure S1I). One obvious reason for this trend is that both NDR length and proportion increase when we engineer three instead of two group 2 motifs. When comparing sequences containing the same motif number, we observe low correlation between NDR length and proportion for group 1 NDFs (Pearson correlation $r = 0.30$ for motif number = 1) and higher correlations for group 2 NDFs ($r = 0.59$ and 0.49 for motif number = 2 and 3, respectively). These data indicate that NDR length and proportion can be individually regulated, but among factors with weaker nucleosome invasion activities (group 2), stronger binding may lead to both higher NDR proportion and longer NDR length.

Differential responses to RSC depletion among NDRs

To test the hypothesis that NDFs can recruit CRs to modulate NDR sizes, we next investigated the change of NDRs in the absence of a CR. If certain NDFs have specificity toward a CR, we expect to see higher responses to CR depletion in comparison with other NDFs and/or TetR. RSC complex is an SWI/SNF family CR that is essential for budding yeast viability. It is highly abundant in yeast and widely associated with promoters (Cairns et al., 1996; Ng et al., 2002; Yen et al., 2012). RSC functions as a nucleosome “pusher” by sliding nucleosomes away from the center of NDRs, and the depletion of RSC reduces genome-wide NDR sizes (Cakiroglu et al., 2019; Harada et al., 2016; Hartley and Madhani, 2009; Klein-Brill et al., 2019; Kubik et al., 2019; Parnell et al., 2008). RSC can directly bind to two DNA motifs, a CG dinucleotide repeat and poly A/T stretch (Cakiroglu et al., 2019; de Boer and Hughes, 2012; Hartley and Madhani, 2009; Zhu et al., 2009). It was also proposed that RSC may be targeted through physical interactions with sequence-specific TFs, e.g., Reb1 (Hartley and Madhani, 2009). However, more recent studies suggest that RSC acts independently of Abf1, Reb1, and Rap1 (Kubik et al., 2018, 2019). Therefore, the mechanism of RSC recruitment, especially over sequences that do not contain RSC-binding motifs, requires further elucidation.

We anchored away GFP-labeled Sth1, the ATPase subunit of RSC, and confirmed the nuclear depletion using fluorescence microscopy (same for other CRs; Figures S2A and S2B). We then mapped nucleosome positioning using the same methyltransferase-based assay described above. On the background sequence, Sth1 depletion causes a slight shift and dephasing of the nucleosome −1 to −7 array, but the overall positioning is largely intact (Figures S2C and S2D). For sequences containing NDF motifs, Sth1 depletion generally leads to NDR shrinkage, consistent with the role of RSC as a nucleosome pusher. One example is shown in Figures 2A and 2B, where the depletion of Sth1 reduces the average NDR size near the Reb1 motif from 247 bp to 157 bp, but the change in NDR proportion is much smaller (from 88% to 81%). Consistently, MNase assay on the same sequence shows NDR shrinkage at the population level, but the nucleosome occupancy near the Reb1 motif

is not affected, indicating that Reb1 can still access its motif in the absence of RSC (Figure 2B). Similar nucleosome occupancy change was observed when Reb1 motif was placed in nucleosome −5, suggesting that the nucleosome invasion by Reb1 with or without Sth1 is not specific to nucleosome −4 (Figure S2E).

The effect of Sth1 depletion is summarized in Figure 2C, where it induces bigger changes in NDR length than NDR proportion (Figure 2D and Table S2). As exceptions, Sth1 depletion lowers NDR proportion for NDRs containing Azf1, Ecm22, Rsc3, Rgt1, Sfp1, and Sut1 motifs (Figure 2C). All of these motifs contain poly A/T or multiple CG dinucleotides that can be recognized by RSC (Figure S2F). These results suggest that RSC can initiate NDR formation by directly binding to these motifs, and RSC depletion reduces NDR proportion in these cases; with other motifs, RSC is recruited after NDF invasion so that it selectively modulates NDR length but not proportion.

When we binned NDRs by size (in the −Sth1 condition) and calculated the average length change for each bin, we noticed a length dependence of the RSC effect. In particular, there is a sharp transition near ~100 bp, where short NDRs ~100 bp are much less affected by Sth1 than medium-sized ones (120–200 bp) (Figure 2E). This trend also applies to NDRs generated by TetR: NDRs containing two *tetO* sites have larger responses to Sth1 depletion than a shorter one containing a single *tetO* (green dots in Figure 2F), suggesting that such length dependence is not dictated by specific interactions between RSC and NDFs, but reflects how RSC engages DNA. As indicated by previous biochemical studies, RSC binding requires ~50 bp of extra-chromosomal DNA (Brahma and Henikoff, 2019; Wagner et al., 2020). With NDF(s) bound in the middle, it is conceivable that only NDRs that are longer than 100 bp can accommodate RSC binding. RSC generates the largest extension for NDRs between 100 and 175 bp, and such effect is reduced for longer NDRs (Figure 2E). For example, extra-long NDRs generated by Ino4 do not shrink in the absence of Sth1 (confirmed by MNase assay, Figure S2G).

The data above indicate that different responses to Sth1 depletion among NDRs are partially due to NDR length. Does RSC have factor specificity *beyond* such length dependence? To address this question, we used the average length-dependence curve as a baseline and examined if NDRs generated by any NDF show responses that significantly deviate from this baseline (STAR Methods). NDRs formed by three factors, Abf1, Reb1, and Sfp1, tend to shrink more than other NDFs in the absence of RSC (red dots in Figure 2F). Since the NDR with two *tetO* sites shrinks to a comparable extent, it is unlikely that this larger effect is due to specific interactions between RSC and these factors. Rather, we suspect that these factors (at least Abf1 and Reb1) bind DNA tightly and compete with nucleosomes effectively, and therefore create more chances for RSC to bind and remodel. In contrast, NDRs generated by a few NDFs, including Bas1, Mcm1, Sum1, and Stp1, are not very sensitive to Sth1 depletion (blue dots in Figure 2F). We noticed that some of these factors, like Bas1 and Mcm1, show high-level protection around their binding sites (Figure S2H). Therefore, we suspect that these NDFs recruit some co-factors to occupy nearby NDRs, leaving little space for RSC to bind and act.

Ino4, Stb5, and Tea1 recruit SWI/SNF to generate extra-long NDRs

We next focused on the SWI/SNF complex. RSC and SWI/SNF belong to the same CR family, and the two complexes show similar nucleosome remodeling activity *in vitro* (Dechassa et al., 2010; Harada et al., 2016; Kassabov et al., 2003; Li et al., 2019; Liu et al., 2011; Lorch et al., 2006; Zhang et al., 2006; Zofall et al., 2006). However, depletion of the catalytic subunits of these two complexes, Sth1 in RSC and Snf2 in SWI/SNF, results in distinct chromatin and gene expression phenotypes. The depletion of Snf2, but not Sth1, strongly inhibits induction of M.CviPI transgene expression and therefore DNA methylation (Figure S3A), which prevents accurate mapping of nucleosomes. To solve this problem, we constructed a second doxycycline-inducible system combining a stronger promoter with a stronger TetR′ activator (Figure S3B), which is much less affected. The stronger induction of this system allows us to get similar levels of methylation in Snf2-depleted cells as in WT cells (Figure S3C).

Since SWI/SNF was categorized as a nucleosome “pusher” that enlarges NDR sizes (Dechassa et al., 2010; Kubik et al., 2019; Kundu et al., 2007; Qiu et al., 2016; Rawal et al., 2018), we expected to detect shorter NDRs upon Snf2 depletion. Surprisingly, most NDRs are unaffected or even slightly lengthened in the absence of Snf2, e.g., the NDR containing Reb1 (Figures 3A, 3B, and 3E). NDRs generated by four NDFs, Ino4, Sfp1, Stb5, and Tea1, show significant shortening upon Snf2 depletion, and two of these cases were confirmed with MNase assay (Figures 3C, 3D, and S3D). Interestingly, three of these four factors, Ino4, Stb5, and Tea1, produce unusually long NDRs (~400 bp) in WT cells (Figure 1G). After Snf2 depletion, the NDRs of these factors drop to ~300 bp, much closer to the average NDR length (225 bp in −Snf2 cells). This result indicates that these extra-long NDRs are generated by SWI/SNF remodeling. Note that not all ~300-bp NDRs are extended by SWI/SNF; in fact, when averaged among NDRs within different length bins, the Snf2 effect does not show strong length dependence (Figure 3F). We therefore conclude that Ino4, Stb5, and Tea1 specifically recruit SWI/SNF to form extra-long NDRs. The Ino4 result is consistent with a previous report that SWI/SNF remodels nucleosomes over the *INO1* promoter, and SWI/SNF recruitment relies on the Ino2/Ino4 activator (Ford et al., 2008).

Ume6 and Rfx1 recruit ISW2 to generate extra-short NDRs

We applied the same analysis to ISW2 depletion. ISW2 slides nucleosomes in the opposite direction of RSC and SWI/SNF, and has nucleosome-spacing activity against a barrier (Fazzio et al., 2001; Kubik et al., 2019; Yen et al., 2012). Depletion of ISW2 lengthens a small fraction of NDRs in the genome (Kubik et al., 2019). Previous studies revealed that ISW2 can be recruited by Ume6 to compact the neighboring nucleosomes (Donovan et al., 2021; Goldmark et al., 2000). ISW2 also showed physical interactions with Cbf1 and Rfx1 (Gavin et al., 2002; Shetty and Lopes, 2010; Zhang and Reese, 2004) and positive genetic interactions with Bas1, Cbf1, and Rap1 (Collins et al., 2007; Costanzo et al., 2016; Zheng et al., 2010). It is not clear if these factors function like Ume6 to target ISW2 to specific chromosome loci and generate localized nucleosome repositioning.

Consistent with previous findings, our data show that Isw2 depletion significantly lengthens the NDRs generated by Ume6 (from 98 bp to 199 bp), which was confirmed by MNase

assay (Figures 4A and 4B). The NDR proportion on this sequence remains the same (both ~68%). This result can also explain our previous finding that the DNA binding domain of Ume6, which lacks the ISW2 interaction domain, generates a longer NDR than full-length Ume6 (Yan et al., 2018) (Figure S4). Interestingly, a similar effect was observed with Rfx1 (Figures 4C and 4D), but not with other NDFs that have been proposed to interact with ISW2, i.e., Cbf1, Rap1, and Bas1 (Figure 4E and Table S2). The rest of NDRs are lengthened slightly in the absence of Isw2, and this effect on average increases linearly with the NDR length (Figure 4F). Comparison with this baseline reveals that Ume6 and Rfx1 are the only outliers (Figure 4G). Overall, these data suggest that ISW2 is specifically recruited by Ume6 and Rfx1 and remodels nucleosomes into NDRs. ISW2 also functions on NDRs that do not contain these factors, but the effect is much weaker. The nonspecific effect increases with NDR length, which indicates that the amount of exposed DNA may contribute to ISW2 recruitment.

INO80 nonspecifically shrinks most NDRs

INO80 complex moves nucleosomes in the same direction as ISW2, and they have redundant functions in modulating NDR sizes (Kubik et al., 2019; Oberbeckmann et al., 2021; Udugama et al., 2011; Yen et al., 2012). Depletion of Ino80, the ATPase subunit of the INO80 complex, lengthens a fraction of genome-wide NDRs (Kubik et al., 2019; Yen et al., 2012). Our measurement also detected NDR size increases in the absence of Ino80. Interestingly, unlike the other CRs that reposition NDR-flanking nucleosomes, Ino80 depletion mostly affects the occupancy of those nucleosomes. One example is shown in Figures 5A and 5B, where Ino80 depletion reduces the occupancy of nucleosomes near a Reb1 site without significantly changing their positions, an effect confirmed by MNase assay (Figure 5B). We also tested a sequence containing three Rgt1 motifs and reached the same conclusion (Figure S5). This point is further illustrated in Figure 5C, where we plotted the histograms of the position and the occupancy change of nucleosome −3 (the nucleosome immediately downstream the NDR) upon the depletion of CRs. The histograms show that Ino80 depletion leads to reduced occupancy of nucleosome −3 but little change in its location, an effect that is unique among the CRs. This observation indicates that INO80 can stabilize NDR-proximal nucleosomes and prevent their eviction, and therefore helps to maintain shorter NDR sizes.

We next investigated the length dependence and factor specificity of INO80 function. The effects on NDR length and proportion for individual NDFs are shown in Figure 5D (Table S2). The effect of Ino80 depletion has a clear length dependence, where the longer NDRs are shortened more efficiently (Figure 5E). This result agrees well with previous observations that the Arp8 and Nhp10 modules of INO80 interact extensively with flanking DNA, and that the INO80 remodeling rate *in vitro* is drastically increased when the flanking DNA exceeds ~50 bp (Eustermann et al., 2018; Knoll et al., 2018; Oberbeckmann et al., 2021). Beyond the length dependence, we did not find any NDFs that consistently show far-from-average responses to Ino80 depletion, indicating that INO80 has little or no specificity toward NDFs. In comparison with ISW2, the nonspecific NDR compaction caused by INO80 is stronger, and indeed, the depletion of Ino80 has larger effect on genome-wide NDRs than ISW2 (Kubik et al., 2019).

Binding and nucleosome invasion of NDFs do not require CRs

Figure 6A summarizes the impact of RSC, SWI/SNF, ISW2, and INO80 depletion on the NDR length and proportion generated by each NDF (averaged among the sequences containing the same NDF motif[s]). In general, the depletion of CRs has larger effect on NDR length than proportion, indicating that NDFs can still bind to their motifs in the absence of CRs. To directly test this idea, we performed chromatin immunoprecipitation (ChIP) on TAP-tagged Reb1 and Ume6 in the presence or absence of RSC and ISW2, respectively. There is no significant change in Reb1 binding with or without Sth1 (Figure 6B). Ume6 binding even increases upon Isw2 depletion (Figure 6C), presumably because the lengthened NDR can accommodate more factors. These data are consistent with our hypothesis that NDFs do not require CRs to bind.

The experiment above depletes CR when Reb1 and Ume6 are pre-bound to their recognition motifs, and the results show that their binding can be *maintained* in the absence of CRs. However, it is still possible that CRs may affect the initial binding of NDFs and the *establishment* of NDRs. For example, the invasion into a nucleosome by an NDF may be slower in the absence of RSC, given that the nucleosome is less mobile. To test this possibility, we constructed a strain containing Sth1 anchor-away and Cbf1 deletion (Cbf1 is chosen because it is the only non-essential NDF in group 1), as well as induced Cbf1 expression by methionine depletion. Methionine depletion by itself does not affect nucleosome occupancy on *HO* promoter (Figure S6A). We then induced Cbf1 in this strain +/− Sth1 and used MNase to measure the nucleosome occupancy over the Cbf1 binding site over time (STAR Methods). Sth1 anchor-away does not have a strong effect on Cbf1 induction level (Figure S6B). We observed gradual displacement of nucleosome −4 away from its initial position with essentially the same rate with or without Sth1 (Figures 6D and 6E). ChIP measurement also shows that Sth1 depletion does not significantly affect the binding rate of Cbf1 to this region (Figure 6F). Overall, these data support the model that during NDR formation, NDF binds DNA and invades into nucleosomes first, and CRs act downstream to reposition the nucleosomes.

Genome-wide analyses of CR effect support the findings from the ISO library

To corroborate the findings on the synthetic sequences above, we investigated the CR effect on nucleosome positioning in the native yeast genome based on published datasets (STAR Methods) (Kubik et al., 2018, 2019). Given our observations that CRs function downstream of NDF binding, we predicted that CR depletion would only affect the NDR sizes without altering the nucleosome occupancy inside the NDR. This is indeed the case for ISW2, INO80, and SWI/SNF, either at a genome-wide scale (Figure S7A) or for the subset of NDRs that are affected by the depletion of these CRs (Figure 7A bottom panels, Table S3). RSC, on the other hand, affects nucleosome occupancy within genome-wide NDRs (Figure S7A). We reasoned that this is because RSC can directly bind to CG-rich or poly A/T sequences and function as a sequence-specific NDF, and in that case, RSC depletion can reduce or even eliminate NDRs. In the absence of these sequences, RSC should function downstream of other NDFs, and it will only affect NDR size. To test this idea, we used recently published ChIP-exo data (Rossi et al., 2021) to divide the genome-wide NDRs into RSC-only, RSC + other NDFs, and other NDFs-only categories (Table S3). For all three

scenarios, NDR sizes decrease upon RSC depletion, but the increases in the nucleosome occupancy are much higher for the first two cases (Figure 7A). These data support our conclusion that except for direct binding of RSC to its consensus motifs, CRs function downstream of NDFs to modulate NDR length, but not NDR proportion.

We next examined the length dependence of the CR function. In Figure 7B, we plotted the NDR size change (WT – CR mutant) versus – CR NDR size, either for individual NDRs (upper panels), or averaged among different size bins (lower panels). Due to the bulk-averaging nature of the genome-wide data, NDR size is calculated in a different way from the single-molecule data (STAR Methods). In addition, when two NDRs are close together, the length change of one may impact another, so not all length changes are direct effects from CR mutations. Despite these issues, the overall trend of length dependence is largely consistent with our conclusions from the ISO library. More specifically, RSC effect decreases over NDR length; SWI/SNF leads to long extension of a small number of NDRs and does not have obvious size dependence; ISWI and INO80 effects slightly increase with NDR length. Unlike the library that is inserted into the same sequence background, genome-wide NDRs have different sequence contexts. Similar length dependence in these two cases indicate that length itself is an important NDR property that contributes to CR function.

Last, we used the genome-wide data to investigate NDF-CR specificity. We collected CR-sensitive NDRs and calculated the enrichment of each NDF in these NDRs based on published ChIP data (STAR Methods). Consistent with our findings above, SWI/SNF and ISW2 have stronger NDF specificity than RSC and INO80 (Figure 7C). Also, Ume6 and Rfx1 are highly enriched in ISW2-affected NDRs, and Tea1 and Stb5 (albeit to a lesser extent) are enriched in SWI/SNF-affected NDRs (too few Ino4 ChIP-sequencing peaks were identified to draw statistical conclusions). However, this analysis also revealed a few other enriched factors, i.e., Bas1 and Sut1 tend to be associated with NDRs that are affected by ISW2, and Leu3, Rsc3, Stp1, and Sut1 with the ones that are affected by SWI/SNF. Interestingly, Bas1 binding is highly correlated with Rfx1: 30 of 95 Bas1 binding sites co-localize with Rfx1 in genome-wide NDRs, and 6 of 10 co-localize in the ISW2-affected NDRs ($p = 10^{-9.9}$ and $10^{-2.0}$, respectively, in comparison with a model in which the two factors are randomly located in NDRs) (Figure S7B). In fact, among all NDFs, Bas1 shows the highest level of co-localization with Rfx1. We therefore suspect that the enrichment of Bas1 in ISW2-affected NDRs is due to its co-binding with Rfx1. We also found statistically significant co-binding between Stp1/Rsc3 and Stb5 (Figure S7B), which may partially explain their enrichment in Snf2-sensitive NDRs.

DISCUSSION

In this work, we systematically investigated the coordination between NDFs and CRs. We used a method that combined synthetic DNA oligo library, accessibility of chromatin to a DNA methyltransferase, and high-fidelity CCS PacBio bisulfite sequencing to measure nucleosome positioning over DNA engineered into the yeast genome in a high-throughput manner. In comparison with more widely used cleavage-based methods, such as DNase I, MNase, and transposase, the methyltransferase-based method allows us to map consecutive

nucleosomes over 1 kb. Because of the single-cell nature of this measurement, we can extract NDR length and proportion separately, which provides critical insights for the interplay between NDFs and CRs.

Nucleosome mapping through methylation readout has some other differences from cleavage-based methods like MNase. The latter allows the size selection of DNA fragments with mono-nucleosome length, and the mapping of these fragments predominantly reflects nucleosome footprints. In contrast, protection from methylation can result from many DNA-binding proteins, including histones, TFs, and CRs. As a consequence, we occasionally observed footprints of unknown nature that lead to protection patterns distinct from those measured by the MNase assay (Figure 3D). Also, MNase is typically applied for a few minutes and therefore provides a “snapshot” of the nucleosome configuration, whereas the methyltransferase is induced for 2 h, and dynamic changes of nucleosomes during that time can be recorded by methylation. For example, we tend to see higher protection of nucleosomes −6 and −5 than nucleosomes −3 to −1, which likely reflects higher dynamics in the downstream nucleosomes. Finally, the resolution of M.CviPI nucleosome mapping is ultimately determined by the density of GC dinucleotides. In the future, this may be further improved by using methyltransferases that target a single nucleotide, e.g., adenine methyltransferase. However, an analogous, high-throughput method of measuring methylation in amplicons is less well-established for A methylation.

Lacking sequence-specific binding domains (except for RSC3), CRs are thought to have both nonspecific activities (e.g., to space nucleosomes across the genome) and localized activities at specific chromatin target sites. These two activities may allow CRs to function both upstream and downstream of NDF binding: CRs may nonspecifically reposition or even evict nucleosomes, allowing transient exposure of otherwise embedded binding sites that can be recognized by NDFs or PFs. Alternatively, NDFs or PFs may first gain access through other mechanisms and then recruit CRs to these regions, allowing them to remodel local nucleosomes. We found that (1) CRs mainly affect NDR length, not NDR proportion, and (2) NDF binding and nucleosome invasion rate are not affected by CR depletion. These results strongly support the model that CRs function downstream of NDF binding and do not play a deterministic role in the initial targeting of NDFs. These results are consistent with the finding that simultaneous depletion of many CRs in yeast does not eliminate NDRs on the native genome (Kubik et al., 2019). It is still unclear how NDFs gain access to their binding sites in the first place, and more studies are needed to address this question.

Our results also provided insights into the mechanism of CR targeting specificity. Despite previous evidence that CRs may be recruited through sequence-specific DNA-binding factors, the specificity between TFs and CRs has not been examined systematically. In addition, it is often difficult to differentiate genome-wide nonspecific CR effect from a more targeted effect. Here, we investigated such specificity by comparing the CR effect on NDRs generated by different NDFs in the same chromatin context. We also included a bacteria TF, TetR, in this comparison, which can form an NDR but is unlikely to have any special interactions with CRs. We found two types of CR-TF specificity. One is between ISW2 and Ume6 or Rfx1. The interaction between ISW2 and Ume6 is well documented, and in particular, an alpha-helical domain on Ume6 contacts the Itc1 subunit of the ISW2

complex (Donovan et al., 2021; Goldmark et al., 2000). Less is known about the interaction between Rfx1 and ISW2, although Rfx1 was shown to work with ISW2 to position a nucleosome array over the *RNR3* promoter (Zhang and Reese, 2004). The other type of CR-TF specificity is between SWI/SNF with Ino4, Stb5, and Tea1. Given a previous report that SWI/SNF can bind to an acidic activation domain (Neely et al., 1999), it is possible that SWI/SNF is recruited by the activation domains of these factors. Detailed interaction mechanism here requires further investigation. The recruitment of SWI/SNF leads to extensive nucleosome remodeling and exposure of long-stretch of nearby DNA. This could explain why SWI/SNF is critical in activating certain genes (e.g., *GAL1* and *HO*) where multiple nucleosomes need to be displaced to expose the core promoter.

In other NDF-CR combinations, NDFs can also have variable responses to CR deletion. One major cause of this variation is NDR size. Both RSC and INO80 were shown to interact extensively with extra-nucleosomal DNA, and such interactions are critical for their remodeling activities. Consistently, we found that short NDRs, generated by either native NDFs or a single TetR, are not significantly affected by these two CRs. Such a length requirement can explain why RSC and INO80 preferentially bind to promoters with extended NDRs instead of canonically sized linker DNA. Previous studies proposed that RSC is recruited by CG-rich and poly A/T motifs, and INO80 is also attracted by poly A·T sequences with high rigidity, i.e., low bending propensity (Badis et al., 2008; Krietenstein et al., 2016; Lorch et al., 2014). It should be noted that most sequences used in our study do not contain these motifs (exceptions listed in Figure S2F). Therefore, while these motifs may contribute to the recruitment of RSC and INO80, they are not required for these CRs to function. ISW2 also has nonspecific effects over NDRs that scale over NDR sizes. Overall, these data suggest that RSC, INO80, and ISW2 can be targeted to promoters by naked DNA that is initially exposed through NDF binding.

With the insights above, we also carried out analyses of genome-wide impact of CR depletion on NDRs. Remarkably, despite the diversity of underlying sequences and TF association in native NDRs, the genome-wide analyses generally support the conclusions drawn from the ISO library. There are a few NDFs that show little response to CR depletion in the ISO library, but were found to be highly enriched among CR-affected native NDRs. This may be due to co-binding of these factors with other factors that recruit the CRs, like the case of Bas1 and Rfx1. Especially for the few factors that are enriched in SWI/SNF-affected NDRs, we suspect that they co-bind with transcription activators that recruit SWI/SNF but are not included in our NDF library. This illustrates the power of the ISO method that allows us to investigate one factor at a time.

Limitations of the study

Our study has two major limitations. First, as we mentioned in the discussion, the accuracy of nucleosome mapping is limited by the density of GCs, and we cannot distinguish the footprints of nucleosomes from other large complexes. Second, we only depleted one CR at a time, and we may underestimate its effect if there is redundancy with other CRs.

STAR★METHODS

RESOURCE AVAILABILITY

Lead contact—Further information and requests for resources and reagents should be directed to and will be fulfilled by the Lead Contact, Lu Bai (lub15@psu.edu).

Materials availability—Requests for yeast strains should be directed to Lu Bai (lub15@psu.edu). Requests for methylation transferase expression plasmids should be directed to Michael Kladde (kladde@ufl.edu). This study does not generate any new reagents.

Data and code availability

Statement about the Data: Raw and processed data generated in this study are available at Gene Expression Omnibus (GEO) under accession number GSE199812. Previously published data that were used in this study are available at GEO: GSE115412 (MNase-seq) and GSE147927 (ChIP data).

Statement about the Code: Code is available at https://github.com/HengyeChen/Pacbio_Data_Analysis (https://doi.org/10.5281/zenodo.6819631).

General statement: "Any additional information required to reanalyze the data reported in this paper is available from the lead contact upon request."

EXPERIMENTAL MODEL AND SUBJECT DETAILS

Yeast strains—Standard methods were used for yeast strain construction. All strains used in this study are derived from w303 background strains. For anchor-away strains, DNA containing FRB-TAP-GFP, FRB-TAP, or FRB-GFP was PCR amplified with primers homologous to the 3′ end of target genes, and the PCR products were inserted to the 3′ end to generate a fusion protein containing FRB. For methylation, we integrated an M.CviPI gene driven by an engineered core *GAL1* promoter that is transcriptionally induced by 17β-estradiol (Jessen et al., 2004, 2006). For Snf2 anchor-away strain, we constructed an alternative, doxycycline-induced system capable of sustaining similar levels of M.CviPI as WT (Figure S3B). The alternative system bypasses transcriptional defects upon Snf2 depletion by enlisting high-level expression of a strong activator with a compound activation domain that recruits 'excess' coactivators to establish functional redundancy (Dhasarathy and Kladde, 2005). Specifically, TetR and reverse TetR (TetR′) were used as DNA binding domains and fused in frame to general repressor Ssn6 and a synthetic compound VP16-Gal4 activation domain (VP16AD-Gal4AD), respectively (Figure S5B). These two proteins were driven by a strong and constitutive promoter, *TDH3pr*. The M.CviPI target gene was driven by an engineered core *CYC1pr* containing seven *tetO* sites. Therefore, M.CviPI expression was repressed by TetR-Ssn6 in the absence of doxycycline. In the presence of doxycycline, TetR-Ssn6 dissociates, and TetR′-VP16AD-Gal4AD binds to 7x*tetO-CYC1pr* to activate the target gene. The strain with inducible Cbf1 was constructed by first inserting a truncated Cbf1 (1–196 amino acids) driven by *GAL1pr* in the endogenous Cbf1 (to eliminate endogenous Cbf1 expression in glucose), and then integrating a Cbf1-TAP driven

by *MET3pr* into the *HIS3* locus. All strains and primers used in this study are listed in Table S4.

METHOD DETAILS

Plasmid library construction—Twenty-nine NDF motifs identified in our previous work were used in library design (Yan et al., 2018). Part of the sequences in nucleosome −4 of the *HO* promoter was replaced by one group 1 NDF motif or two to three group 2 NDF motifs (no change in the overall length). The final length of oligos is 160 bp, including part of nucleosome −4 that contains the various NDF motifs, eight-base-pair barcodes upstream of the variable region, two BbsI cutting sites between the barcode and variable region, and two BsaI cutting sites at the ends of the oligo. The backbone plasmid contains an engineered *HO* promoter in which the region between −1176 bp and −685 bp was deleted with two BbsI cutting sites inserted in between. The plasmid library was constructed by a two-step insertion. First, the backbone plasmid was digested by BbsI and ligated to the oligo library digested by BsaI to generate plasmid library 1. Plasmid library 1 was cut by BbsI again, and a sequence containing part of the −7, −6, and −5 nucleosomes was inserted into library 1 to construct the final library.

ISO library construction: The plasmid library was linearized by ApaI to integrate into the *CLN2* locus. Anchor-away strains were cultured in 250 mL YEPD to OD_{660} of 0.7. Cells were pelleted by centrifugation and washed with 50 mL of distilled deionized H_2O (ddH_2O) and 1xLiAc/TE (1.02 g/mL LiAc, 10 mM Tris, pH 8.0, and 1 mM EDTA, pH 8.0). The cell pellet was then resuspended in equal volume of 1xLiAc/TE. Each 2 mL of yeast suspension was mixed with 6 mg carrier DNA, 20 mL of 1xLiAc/TE + 40% PEG 8000, and 20 μg of linearized library in a 50 mL conical tube. The mixture was vortexed for 60 s, incubated at 30°C for 30 min, and then at 42°C for 30 min. After incubation, cells were washed with ddH_2O twice, and then resuspended in 10 mL of D-Ura medium. Cell suspension (100 μL) was plated on D-Ura plates with serial dilution to measure the transformation efficiency. Usually, 10,000 to 20,000 colonies were obtained from 250 mL of yeast culture. The rest of the cell suspension was transferred to 1 L of D-Ura medium and cultured for two days at 30°C. Cells were then harvested for experiment or storage.

M.CviPI expression induction: One mL of frozen yeast library was thawed and added into 1 L of SCD-Ura medium followed by overnight incubation at 30°C. The yeast library was then re-inoculated into 250 mL of D-Met-Ura medium and cultured overnight at 30°C. Pre-cultured yeast library was diluted to OD_{660} of 0.05 using 160 mL of D-Met-Ura medium and incubated at 30°C until OD_{660} was 0.2. Yeast culture (160 mL) was divided into two flasks and incubated with (1 μg/mL) rapamycin and (1/5000th volume) dimethylsulfoxide vehicle, respectively. 17β-Estradiol was then added to all flasks (final concentration 100 nM); cells were cultured for two more hours and then harvested.

Bisulfite PacBio amplicon sequencing: After harvesting, cells were washed twice using ddH_2O, transferred into a 1.5 mL tube, and resuspended in 1 mL spheroplasting solution (1 M sorbitol, 0.5 mM β-mercaptoethanol). Ten microliters of 10 mg/mL Zymolyase 100T was added to each tube, and the tubes were incubated at 37°C for 30 min with rolling.

Spheroplasts were pellet by centrifugation and resuspended in 400 μL TE buffer, pH 8.0. Lysis buffer (100 μL; 0.28 M EDTA, pH 8.0, 0.22 M Tris-HCl, pH 8.0, and 2.2% sodium dodecyl sulfate (SDS)) was added to each tube and then incubated at 65°C for 30 min. DNA was then extracted with 400 μL of phenol:chloroform:isoamyl alcohol (25:24:1) and precipitated with 750 μL ethanol. The DNA pellets were resuspended in 400 μL of TE buffer, pH 8.0 and digested with 0.75 mg/mL RNase A. One milliliter of ethanol and 15 μL of 2 M ammonium acetate were added to precipitate DNA. The DNA pellet was washed with 1 mL of 70% ethanol and resuspended in 100 μL TE buffer, pH 8.0. DNA samples were then purified using Omega Cycle Pure kit.

Bisulfite conversion of methylated genomic DNA was done with EpiTect Fast DNA Bisulfite kit. Bisulfite-converted DNA was then amplified by EpiMark Hot Start Taq DNA Polymerase and Turbo Cx Pfu for 23 cycles. A 25 μL PCR reaction contained 1 μL of bisulfite-converted template, 0.5 μL of each 10 μM primer, 5 μL of 5x EpiMark Taq buffer, 0.5 μL of 10 mM dNTPs, 0.125 μL (0.625 unit) of EpiMark Hot Start Taq DNA Polymerase, and 0.05 μL (0.125 unit) of Pfu Turbo Cx HotStart DNA polymerase. PCR reactions were concentrated using Amicon Ultra 30K filters and then purified using SPRI beads. PCR amplicons were sequenced by PacBio Sequel system. The sequencing service was provided by University of Florida's Interdisciplinary Center for Biotech Research (ICBR) and the Pennsylvania State University (PSU) Genomics Core Facility.

MNase assay: We followed a previously described protocol (Bai et al., 2010). Nucleosome occupancy was normalized to a well-positioned nucleosome in the terminator of *EX O 84*.

ChIP: The ChIP protocol was modified from a previously described procedure (Du et al., 2019). Yeast strains were grown to OD_{660} of 0.4 in 50 mL of D-Met medium and crosslinked with 1.39 mL of 37% formaldehyde for 20 min at room temperature. Crosslinking was quenched by adding 2.7 mL of 2.5 M glycine and incubation for 5 min. Crosslinked cells were centrifuged at 1882 × *g* for 3 min at 4°C, and then washed twice with cold 1x Tris-buffer saline (TBS). Cell pellet was then resuspended in 250 μL of fresh FSPP buffer (50 mM HEPES-KOH, pH 7.5, 140 mM NaCl, 1 mM EDTA, 1% Triton X-100, 0.1% sodium deoxycholate, 1% protease inhibitor cocktail, and 1 mM phenylmethylsulfonyl fluoride (PMSF) and vortexed with ~300 μL glass beads for 2 cycles of 20 min with an intervening 10 min in a 4°C cold room. Another 250 μL of fresh FSPP was added to each sample, and the cap and bottom of tubes were punched with a hot needle so that cell lysate could be collected by centrifuging at 836 × *g* for 5 min at 4°C. FSPP (0.5 mL) was added to the cell lysate to resuspend the pellet. The cell lysate was then sonicated using a 30 s on 30 s off cycle at 4°C for 7 cycles. Sonicated cell lysate was transferred to 1.5 mL tube and centrifuged at 17,136 × *g* for 20 min at 4°C. Two hundred microliters of supernatant was saved as input. Another 200 μL of supernatant was mixed with 800 μL of FSPP buffer and 100 μL of pre-blocked IgG beads. Chromatin was incubated with the beads overnight at 4°C, and then washed sequentially at 4°C with 1xFA-lysis buffer (50 mM HEPES-KOH, pH 7.5, 140 mM NaCl, 1 mM EDTA, 1% Triton X-100, 0.1% sodium deoxycholate), 1xFA-lysis buffer containing 150 mM NaCl, 1xFA-lysis buffer containing 500 mM NaCl, LiCl buffer (0.25 M LiCl, 1% NP-40, 1% sodium deoxycholate, 1 mM EDTA, and 10 mM Tris-HCl

pH 8.0), and lastly TE buffer, pH 8.0. Chromatin was then eluted with 400 μL ChIP elution buffer (50 mM NaCl, 50 mM Tris-HCl, pH 8.0, 10 mM EDTA, 1% SDS). Samples were mixed by rotation at 30°C for 30 min. Beads were pelleted by centrifugation at 17,136 × *g* and discarded. Five microliters of 20 mg/mL Proteinase K was added to supernatant; 180 μL of 1xFA-lysis buffer, 20 μL of 10% SDS and 5 μL of 20 mg/mL Proteinase K were added into the input samples. ChIP and input samples were then incubated overnight at 65°C to reverse crosslinking. DNA was extracted by phenol:chloroform:isoamyl alcohol (25:24:1) followed by ethanol precipitation. Input samples were then treated with 200 μg RNase A and precipitated with ethanol after adding 20 μg glycogen. Enrichments of target TFs were quantified by quantitative PCR (qPCR).

Quantification and statistical analysis

General information about statistical analyses: General statistical analyses were performed using MATLAB and OriginPro. Chi square test was used to calculate the significance of colocalization of NDFs in NDRs in Figure S7B. Student's t-test was used to calculate the significance of TF binding and expression in Figure 6F and S6B. Number of replicates can be found in the figure legends. Significance was set at p value <0.05.

Nucleosome mapping: Consensus sequence (CCS) were generated from PacBio Sequel subreads with at least 3–5 passes. GC and other C in each reference sequence were converted to GY and T, respectively. CCS reads were aligned using MATLAB scripts based on global and local alignment. We removed reads if 1) alignment accuracy is lower than 90%, 2) there is more than one mismatch in the synthetic oligo region (430–540 bp in the reference sequence that contains NDF motifs), 3) there is a mismatch in NDF motifs, or 4) methylation level too low (< four methylated GC in total). The alignment was performed on the PSU Institute for Computational and Data Sciences Roar supercomputer. With a few exceptions, we only included ISO sequences with at least 140 reads for subsequent analysis.

Methylation levels of each sample were normalized to the WT sample to account for the variation in M.CviPI expression. Nucleosomes were predicted on each read based on the space between methylated GCs (Figures S1A–S1C). We assumed that the DNA was fully protected from methylation near the nucleosome pseudodyad but had some flexibility near the entry/exit sites (Figure S1A) (Kladde and Simpson, 1994; Kladde et al., 1996). We correlated this pattern with the methylation measurement in a 147 bp moving window to get a "nucleosome penalty score" and placed nucleosomes at the local minimums (Figure S1B). No nucleosomes were placed in regions with penalty score above 0.5 (Figure S1B). For most NDFs, like Abf1 and Reb1, regions immediately adjacent to their motifs were highly methylated, clearly indicating the presence of NDRs (Figures 1E and 2A). However, for a small number of factors, e.g. Ino4, regions near their motifs were well protected, but the downstream regions were widely open (Figure 3C). For this scenario, we hypothesized that the protection was not generated by nucleosomes, and indeed, MNase experiments revealed extended NDR over the Ino4 motif (Figure 3D). To avoid wrong nucleosome placement in cases like Ino4, we calculated the total methylation level in the "NDR region" of each read (from −958 bp to −405 bp). If this number was higher than those in 90% of the background reads (Figure S1D), we assumed the presence of NDR and removed the

nucleosome covering the NDF motif(s). We then carried out fine-tuning of the nucleosome positioning. When a protected region had a length between mono- and di-nucleosomes, the nucleosome was set as 160 bp and placed at the center of the protected region (Figure S1B). If this lengthy protection was adjacent to an NDF motif, we placed the nucleosome at the edge of this region away from the motif assuming that part of the protection was generated by the NDF, or factors recruited by the NDF. Highly methylated reads (top 5%) were removed when calculating average NDR length to avoid bias generated by a small proportion of very long NDRs. Heatmaps like in Figure 1C were plotted using MATLAB. Radar plots were plotted using Matplotlib.

NDF outlier analysis: NDR length and proportion were calculated on each library sequence in WT and CR-depleted cells (Table S2). Since CR depletion has little effect on NDR proportion, we mostly focused on the change of NDR length. We first binned NDRs based on their length after CR depletion and averaged the ΔNDR (WT – mut CR) in each bin. Depending on how ΔNDR changed with length, we either fit with a straight line, or calculated a smoothed curve (MATLAB “smooth” function) as the length dependence baseline (e.g. in Figure 2E). CR effect on individual ISO sequences was compared with this baseline. Note that our library includes four sequences per NDF, and we only consider a factor as an “outlier” when two or more sequences associated with the same factor show far-from-average behaviors. More specifically, we calculated the difference between each ΔNDR to this baseline (residue). We collected all the data points that fell beyond 1.3 standard deviations on either side. Among these far-from-average data points on each side, if we found two or more corresponded to the same NDF, we called this NDF an outlier as its behavior is significantly different from the rest of the NDFs ($p < 0.01$).

Quantification of MNase time course assay: To quantify the change of nucleosome positioning in the MNase time course (Figure 6D), we calculated the Pearson correlation of nucleosome occupancies between the – Cbf1 condition and each time point. The correlation at different time points was then normalized so that the final correlation is zero (Figure 6E).

Genome-wide analysis: The following genome-wide nucleosome positioning data are used for the analysis here: Sth1 (+/−): GSM2589911/12 (Kubik et al., 2018); Snf2 (+/−): GSM3177770/1; Isw2 (+/−): GSM3177774/5; Ino80 (+/−): GSM3177778/9 (Kubik et al., 2019). NDRs in each of the datasets were computed by an algorithm described previously (Kharerin and Bai, 2021). The CR-sensitive subset was identified based on two criteria: 1) the change in nucleosome occupancy in a 150 bp region centered at the upstream or downstream edge of NDRs should have significant change +/− CRs ($p < 0.01$), and 2) the length of NDR should differ more than 10 bp. The NDFs bound in each NDR in the WT cells were annotated based on ChIP-exo data (Rossi et al., 2021). NDF enrichment was determined by the Chi-square test. The coordinates of NDRs in WT and mutant cells, the CR-sensitive subsets, and NDFs bound in the WT NDRs are listed in Table S3.

Supplementary Material

Refer to Web version on PubMed Central for supplementary material.

ACKNOWLEDGMENTS

We thank Dr. Joseph Reese for providing anchor-away plasmids and yeast strains. We acknowledge all members in the Bai lab for insightful comments on the manuscript. We also thank the members of the Center of Eukaryotic Gene Regulation at Pennsylvania State University for discussions and technical support. This work is supported by the National Institutes of Health (R35 GM139654 to L.B.).

REFERENCES

Badis G, Chan ET, van Bakel H, Pena-Castillo L, Tillo D, Tsui K, Carlson CD, Gossett AJ, Hasinoff MJ, Warren CL, et al. (2008). A library of yeast transcription factor motifs reveals a widespread function for Rsc3 in targeting nucleosome exclusion at promoters. Mol. Cell 32, 878–887. 10.1016/j.molcel.2008.11.020. [PubMed: 19111667]

Bai L, Charvin G, Siggia ED, and Cross FR (2010). Nucleosome-depleted regions in cell-cycle-regulated promoters ensure reliable gene expression in every cell cycle. Dev. Cell 18, 544–555. 10.1016/j.devcel.2010.02.007. [PubMed: 20412770]

Bai L, Ondracka A, and Cross FR (2011). Multiple sequence-specific factors generate the nucleosome-depleted region on CLN2 promoter. Mol. Cell 42, 465–476. 10.1016/j.molcel.2011.03.028. [PubMed: 21596311]

Brahma S, and Henikoff S (2019). RSC-associated subnucleosomes define MNase-sensitive promoters in yeast. Mol. Cell 73, 238–249.e3. 10.1016/j.molcel.2018.10.046. [PubMed: 30554944]

Cairns BR, Lorch Y, Li Y, Zhang M, Lacomis L, ErdjumentBromage H, Tempst P, Du J, Laurent B, and Kornberg RD (1996). RSC, an essential, abundant chromatin-remodeling complex. Cell 87, 1249–1260. 10.1016/S0092-8674(00)81820-6. [PubMed: 8980231]

Cakiroglu A, Clapier CR, Ehrensberger AH, Darbo E, Cairns BR, Luscombe NM, and Svejstrup JQ (2019). Genome-wide reconstitution of chromatin transactions reveals that RSC preferentially disrupts H2AZ-containing nucleosomes. Genome Res 29, 988–998. 10.1101/gr.243139.118. [PubMed: 31097474]

Collins SR, Miller KM, Maas NL, Roguev A, Fillingham J, Chu CS, Schuldiner M, Gebbia M, Recht J, Shales M, et al. (2007). Functional dissection of protein complexes involved in yeast chromosome biology using a genetic interaction map. Nature 446, 806–810. 10.1038/nature05649. [PubMed: 17314980]

Costanzo M, VanderSluis B, Koch EN, Baryshnikova A, Pons C, Tan G, Wang W, Usaj M, Hanchard J, Lee SD, et al. (2016). A global genetic interaction network maps a wiring diagram of cellular function. Science 353, aaf1420. 10.1126/science.aaf1420.

de Boer CG, and Hughes TR (2012). YeTFaSCo: a database of evaluated yeast transcription factor sequence specificities. Nucleic Acids Res 40, D169–D179. 10.1093/nar/gkr993. [PubMed: 22102575]

Dechassa ML, Sabri A, Pondugula S, Kassabov SR, Chatterjee N, Kladde MP, and Bartholomew B (2010). SWI/SNF has intrinsic nucleosome disassembly activity that is dependent on adjacent nucleosomes. Mol. Cell 38, 590–602. 10.1016/j.molcel.2010.02.040. [PubMed: 20513433]

Dhasarathy A, and Kladde MP (2005). Promoter occupancy is a major determinant of chromatin remodeling enzyme requirements. Mol. Cell Biol 25, 2698–2707. 10.1128/MCB.25.7.2698-2707.2005. [PubMed: 15767675]

Donovan BT, Chen H, Jipa C, Bai L, and Poirier MG (2019). Dissociation rate compensation mechanism for budding yeast pioneer transcription factors. Elife 8, e43008. 10.7554/eLife.43008. [PubMed: 30888317]

Donovan DA, Crandall JG, Truong VN, Vaaler AL, Bailey TB, Dinwiddie D, Banks OG, McKnight LE, and McKnight JN (2021). Basis of specificity for a conserved and promiscuous chromatin remodeling protein. Elife 10, e64061. [PubMed: 33576335]

Drouin J (2014). Minireview: pioneer transcription factors in cell fate specification. Mol. Endocrinol 28, 989–998. 10.1210/me.2014-1084. [PubMed: 24825399]

Du M, Kodner S, and Bai L (2019). Enhancement of LacI binding in vivo. Nucleic Acids Res 47, 9609–9618. 10.1093/nar/gkz698. [PubMed: 31396617]

Eustermann S, Schall K, Kostrewa D, Lakomek K, Strauss M, Moldt M, and Hopfner KP (2018). Structural basis for ATP-dependent chromatin remodelling by the INO80 complex. Nature 556, 386–390. 10.1038/s41586-018-0029-y. [PubMed: 29643509]

Fazzio TG, Kooperberg C, Goldmark JP, Neal C, Basom R, Delrow J, and Tsukiyama T (2001). Widespread collaboration of Isw2 and Sin3-Rpd3 chromatin remodeling complexes in transcriptional repression. Mol. Cell Biol 21, 6450–6460. 10.1128/Mcb.21.19.6450-6460.2001. [PubMed: 11533234]

Ford J, Odeyale O, and Shen CH (2008). Activator-dependent recruitment of SWI/SNF and INO80 during INO1 activation. Biochem. Biophys. Res. Commun 373, 602–606. 10.1016/j.bbrc.2008.06.079. [PubMed: 18593569]

Fernandez Garcia M, Moore CD, Schulz KN, Alberto O, Donague G, Harrison MM, Zhu H, and Zaret KS (2019). Structural features of transcription factors associating with nucleosome binding. Mol. Cell 75, 921–932.e6. 10.1016/j.molcel.2019.06.009. [PubMed: 31303471]

Gavin AC, Bösche M, Krause R, Grandi P, Marzioch M, Bauer A, Schultz J, Rick JM, Michon AM, Cruciat CM, et al. (2002). Functional organization of the yeast proteome by systematic analysis of protein complexes. Nature 415, 141–147. 10.1038/415141a. [PubMed: 11805826]

Goldmark JP, Fazzio TG, Estep PW, Church GM, and Tsukiyama T (2000). The Isw2 chromatin remodeling complex represses early meiotic genes upon recruitment by Ume6p. Cell 103, 423–433. 10.1016/S0092-8674(00)00134-3. [PubMed: 11081629]

Harada BT, Hwang WL, Deindl S, Chatterjee N, Bartholomew B, and Zhuang X (2016). Stepwise nucleosome translocation by RSC remodeling complexes. Elife 5, e10051. 10.7554/eLife.10051. [PubMed: 26895087]

Hartley PD, and Madhani HD (2009). Mechanisms that specify promoter nucleosome location and identity. Cell 137, 445–458. 10.1016/j.cell.2009.02.043. [PubMed: 19410542]

Iwafuchi-Doi M, and Zaret KS (2014). Pioneer transcription factors in cell reprogramming. Genes Dev 28, 2679–2692. 10.1101/gad.253443.114. [PubMed: 25512556]

Jeong KW, Andreu-Vieyra C, You JS, Jones PA, and Stallcup MR (2014). Establishment of active chromatin structure at enhancer elements by mixed-lineage leukemia 1 to initiate estrogen-dependent gene expression. Nucleic Acids Res 42, 2245–2256. 10.1093/nar/gkt1236. [PubMed: 24288367]

Jessen WJ, Dhasarathy A, Hoose SA, Carvin CD, Risinger AL, and Kladde MP (2004). Mapping chromatin structure in vivo using DNA methyltransferases. Methods 33, 68–80. 10.1016/j.ymeth.2003.10.025. [PubMed: 15039089]

Jessen WJ, Hoose SA, Kilgore JA, and Kladde MP (2006). Active PHO5 chromatin encompasses variable numbers of nucleosomes at individual promoters. Nat. Struct. Mol. Biol 13, 256–263. 10.1038/nsmb1062. [PubMed: 16491089]

Kassabov SR, Zhang B, Persinger J, and Bartholomew B (2003). SWI/SNF unwraps, slides, and rewraps the nucleosome. Mol. Cell 11, 391–403. 10.1016/s1097-2765(03)00039-x. [PubMed: 12620227]

Kelso TWR, Porter DK, Amaral ML, Shokhirev MN, Benner C, and Hargreaves DC (2017). Chromatin accessibility underlies synthetic lethality of SWI/SNF subunits in ARID1A-mutant cancers. Elife 6, e30506. 10.7554/eLife.30506.001. [PubMed: 28967863]

Kharerin H, and Bai L (2021). Thermodynamic modeling of genome-wide nucleosome depleted regions in yeast. PLoS Comput. Biol 17, e1008560. 10.1371/journal.pcbi.1008560. [PubMed: 33428627]

King HW, and Klose RJ (2017). The pioneer factor OCT4 requires the chromatin remodeller BRG1 to support gene regulatroy element funciton in mouse embryonic stem cells. Elife 6, e22631. 10.7554/eLife.22631. [PubMed: 28287392]

Kladde MP, and Simpson RT (1994). Positioned nucleosomes inhibit Dam methylation in vivo. Proc. Natl. Acad. Sci. USA 91, 1361–1365. 10.1073/pnas.91.4.1361. [PubMed: 8108416]

Kladde MP, Xu M, and Simpson RT (1996). Direct study of DNA-protein interactions in repressed and active chromatin in living cells. EMBO J 15, 6290–6300. [PubMed: 8947052]

Klein-Brill A, Joseph-Strauss D, Appleboim A, and Friedman N (2019). Dynamics of chromatin and transcription during transient depletion of the RSC chromatin remodeling complex. Cell Rep 26, 279–292.e5. 10.1016/j.celrep.2018.12.020. [PubMed: 30605682]

Knoll KR, Eustermann S, Niebauer V, Oberbeckmann E, Stoehr G, Schall K, Tosi A, Schwarz M, Buchfellner A, Korber P, and Hopfner KP (2018). The nuclear actin-containing Arp8 module is a linker DNA sensor driving IN080 chromatin remodeling. Nat. Struct. Mol. Biol 25, 823–832. 10.1038/S41594-018-0115-8. [PubMed: 30177756]

Krietenstein N, Wal M, Watanabe S, Park B, Peterson CL, Pugh BF, and Korber P (2016). Genomic nucleosome organization reconstituted with pure proteins. Cell 167, 709–721.e12. 10.1016/j.cell.2016.09.045. [PubMed: 27768892]

Kubik S, Bruzzone MJ, Challal D, Dreos R, Mattarocci S, Bucher P, Libri D, and Shore D (2019). Opposing chromatin remodelers control transcription initiation frequency and start site selection. Nat. Struct. Mol. Biol 26, 744–754. 10.1038/s41594-019-0273-3. [PubMed: 31384063]

Kubik S, O'Duibhir E, de Jonge WJ, Mattarocci S, Albert B, Falcone JL, Bruzzone MJ, Holstege FCP, and Shore D (2018). Sequence-directed action of RSC remodeler and general regulatory factors Modulates+1 nucleosome position to facilitate transcription. Mol. Cell 71, 89–102.e5. 10.1016/j.molcel.2018.05.030. [PubMed: 29979971]

Kundu S, Horn PJ, and Peterson CL (2007). SWI/SNF is required for transcriptional memory at the yeast GAL gene cluster. Genes Dev 21, 997–1004. 10.1101/gad.1506607. [PubMed: 17438002]

Li M, Xia X, Tian Y, Jia Q, Liu X, Lu Y, Li M, Li X, and Chen Z (2019). Mechanism of DNA translocation underlying chromatin remodelling by Snf2. Nature 567, 409–413. 10.1038/s41586-019-1029-2. [PubMed: 30867599]

Liu N, Peterson CL, and Hayes JJ (2011). SWI/SNF- and RSC-catalyzed nucleosome mobilization requires internal DNA loop translocation within nucleosomes. Mol. Cell Biol 31, 4165–4175. 10.1128/MCB.05605-11. [PubMed: 21859889]

Lorch Y, Maier-Davis B, and Kornberg RD (2006). Chromatin remodeling by nucleosome disassembly in vitro. Proc. Natl. Acad. Sci. USA 103, 3090–3093. 10.1073/pnas.0511050103. [PubMed: 16492771]

Lorch Y, Maier-Davis B, and Kornberg RD (2014). Role of DNA sequence in chromatin remodeling and the formation of nucleosome-free regions. Genes Dev 28, 2492–2497. 10.1101/gad.250704.114. [PubMed: 25403179]

Mueller BU, Pabst T, Osato M, Asou N, Johansen LM, Minden MD, Behre G, Hiddemann W, Ito Y, and Tenen DG (2003). Heterozygous PU.1 mutations are associated with acute myeloid leukemia. Blood 101, 2074. 10.1182/blood-2002-12-3903. [PubMed: 12584148]

Neely KE, Hassan AH, Wallberg AE, Steger DJ, Cairns BR, Wright AP, and Workman JL (1999). Activation domain-mediated targeting of the SWI/SNF complex to promoters stimulates transcription from nucleosome arrays. Mol. Cell 4, 649–655. 10.1016/S1097-2765(00)80216-6. [PubMed: 10549297]

Ng HH, Robert F, Young RA, and Struhl K (2002). Genome-wide location and regulated recruitment of the RSC nucleosome-remodeling complex. Genes Dev 16, 806–819. 10.1101/gad.978902. [PubMed: 11937489]

Oberbeckmann E, Krietenstein N, Niebauer V, Wang Y, Schall K, Moldt M, Straub T, Rohs R, Hopfner KP, Korber P, and Eustermann S (2021). Ruler elements in chromatin remodelers set nucleosome array spacing and phasing. Nat. Commun 12, 3232. 10.1038/s41467-021-23015-0. [PubMed: 34050140]

Parnell TJ, Huff JT, and Cairns BR (2008). RSC regulates nucleosome positioning at Pol II genes and density at Pol III genes. EMBO J 27, 100–110. 10.1038/sj.emboj.7601946. [PubMed: 18059476]

Qiu H, Chereji RV, Hu C, Cole HA, Rawal Y, Clark DJ, and Hinne-busch AG (2016). Genome-wide cooperation by HAT Gcn5, remodeler SWI/SNF, and chaperone Ydj1 in promoter nucleosome eviction and transcriptional activation. Genome Res 26, 211–225. 10.1101/gr.196337.115. [PubMed: 26602697]

Rawal Y, Chereji RV, Qiu H, Ananthakrishnan S, Govind CK, Clark DJ, and Hinnebusch AG (2018). SWI/SNF and RSC cooperate to reposition and evict promoter nucleosomes at highly expressed genes in yeast. Genes Dev 32, 695–710. 10.1101/gad.312850.118. [PubMed: 29785963]

Rossi MJ, Kuntala PK, Lai WKM, Yamada N, Badjatia N, Mittal C, Kuzu G, Bocklund K, Farrell NP, Blanda TR, et al. (2021). A high-resolution protein architecture of the budding yeast genome. Nature 592, 309–314. 10.1038/s41586-021-03314-8. [PubMed: 33692541]

Schick S, Rendeiro AF, Runggatscher K, Ringler A, Boidol B, Hinkel M, Májek P, Vulliard L, Penz T, Parapatics K, et al. (2019). Systematic characterization of BAF mutations provides insights into intracomplex synthetic lethalities in human cancers. Nat. Genet 51, 1399–1410. 10.1038/s41588-019-0477-9. [PubMed: 31427792]

Shetty A, and Lopes JM (2010). Derepression of INO1 transcription requires cooperation between the Ino2p-Ino4p heterodimer and Cbf1p and recruitment of the ISW2 chromatin-remodeling complex. Eukaryot. Cell 9, 1845–1855. 10.1128/Ec.00144-10. [PubMed: 20935143]

Struhl K, and Segal E (2013). Determinants of nucleosome positioning. Nat. Struct. Mol. Biol 20, 267–273. 10.1038/nsmb.2506. [PubMed: 23463311]

Udugama M, Sabri A, and Bartholomew B (2011). The INO80 ATP-dependent chromatin remodeling complex is a nucleosome spacing factor. Mol. Cell Biol 31, 662–673. 10.1128/Mcb.01035-10. [PubMed: 21135121]

van Bakel H, Tsui K, Gebbia M, Mnaimneh S, Hughes TR, and Nislow C (2013). A compendium of nucleosome and transcript profiles reveals determinants of chromatin architecture and transcription. PLoS Genet 9, e1003479. 10.1371/journal.pgen.1003479. [PubMed: 23658529]

Wagner FR, Dienemann C, Wang H, Stützer A, Tegunov D, Urlaub H, and Cramer P (2020). Structure of SWI/SNF chromatin remodeller RSC bound to a nucleosome. Nature 579, 448–451. 10.1038/s41586-020-2088-0. [PubMed: 32188943]

Wang Q, Li W, Liu XS, Carroll JS, Jänne OA, Keeton EK, Chinnaiyan AM, Pienta KJ, and Brown M (2007). A hierarchical network of transcription factors governs androgen receptor-dependent prostate cancer growth. Mol. Cell 27, 380–392. 10.1016/j.molcel.2007.05.041. [PubMed: 17679089]

Xu M, Kladde MP, Van Etten JL, and Simpson RT (1998). Cloning, characterization and expression of the gene coding for a cytosine-5-DNA methyltransferase recognizing GpC. Nucleic Acids Res 26, 3961–3966. 10.1093/nar/26.17.3961. [PubMed: 9705505]

Yan C, Chen H, and Bai L (2018). Systematic study of nucleosome-displacing factors in budding yeast. Mol. Cell 71, 294–305.e4. 10.1016/j.molcel.2018.06.017. [PubMed: 30017582]

Yen K, Vinayachandran V, Batta K, Koerber RT, and Pugh BF (2012). Genome-wide nucleosome specificity and directionality of chromatin remodelers. Cell 149, 1461–1473. 10.1016/j.cell.2012.04.036. [PubMed: 22726434]

Zaret KS, and Carroll JS (2011). Pioneer transcription factors: establishing competence for gene expression. Genes Dev 25, 2227–2241. 10.1101/gad.176826.111. [PubMed: 22056668]

Zhang Y, Smith CL, Saha A, Grill SW, Mihardja S, Smith SB, Cairns BR, Peterson CL, and Bustamante C (2006). DNA translocation and loop formation mechanism of chromatin remodeling by SWI/SNF and RSC. Mol. Cell 24, 559–568. 10.1016/j.molcel.2006.10.025. [PubMed: 17188033]

Zhang Z, and Reese JC (2004). Ssn6-Tup1 requires the ISW2 complex to position nucleosomes in Saccharomyces cerevisiae. EMBO J 23, 2246–2257. 10.1038/sj.emboj.7600227. [PubMed: 15116071]

Zheng J, Benschop JJ, Shales M, Kemmeren P, Greenblatt J, Cagney G, Holstege F, Li H, and Krogan NJ (2010). Epistatic relationships reveal the functional organization of yeast transcription factors. Mol. Syst. Biol 6, 420. 10.1038/msb.2010.77. [PubMed: 20959818]

Zhu C, Byers KJRP, McCord RP, Shi Z, Berger MF, Newburger DE, Saulrieta K, Smith Z, Shah MV, Radhakrishnan M, et al. (2009). High-resolution DNA-binding specificity analysis of yeast transcription factors. Genome Res 19, 556–566. 10.1101/gr.090233.108. [PubMed: 19158363]

Zofall M, Persinger J, Kassabov SR, and Bartholomew B (2006). Chromatin remodeling by ISW2 and SWI/SNF requires DNA translocation inside the nucleosome. Nat. Struct. Mol. Biol 13, 339–346. 10.1038/nsmb1071. [PubMed: 16518397]

Highlights

- Chromatin remodelers (CRs) are dispensable for nucleosome invasion by NDFs
- CRs function downstream of NDF invasion to modulate the sizes of NDRs
- RSC and INO80 mostly bind long NDRs in an NDF-nonspecific manner
- SWI/SNF and ISW2 are specifically recruited by some NDFs

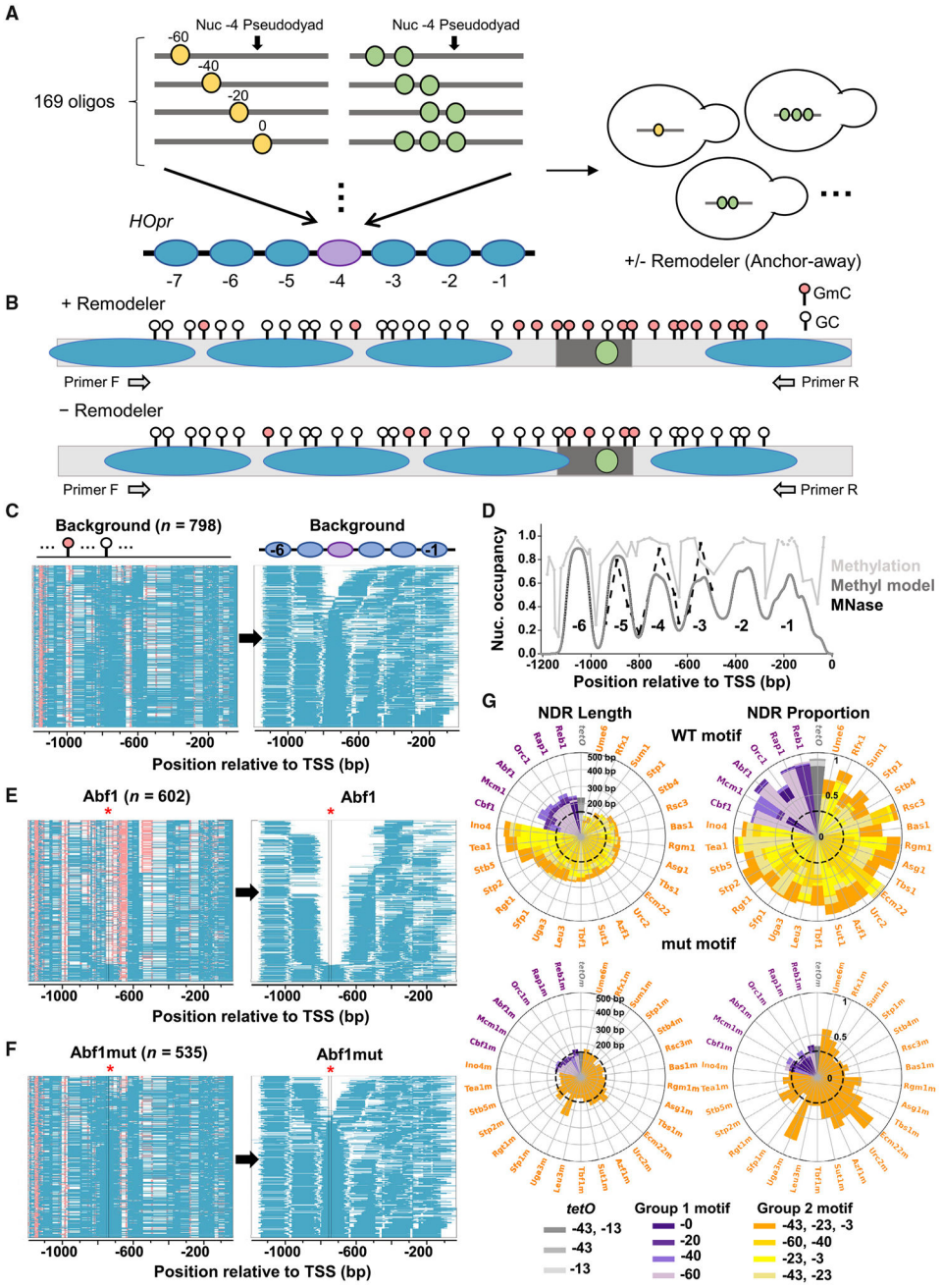

Figure 1. NDFs generate variable nucleosome positioning patterns in WT cells

(A) Construction of the ISO library. We designed an oligo library with 169 oligos, where each oligo contains one to three binding motifs of an NDF. The oligos were ligated into the *HOpr* and integrated into the *CLN2* locus in an anchor-away yeast strain.

(B) DNA methyltransferase-based nucleosome mapping in the presence or absence of remodelers. Nucleosomes on the modified *HOpr* were mapped based on differential methylation in nucleosomes versus open regions.

(C) Methylation (left) and nucleosome positioning (right) on background *HOpr* (no NDF sites). Each row in the heatmap is a single read. Read counts are shown at the top. Red

color represents methylated regions; blue color represents unmethylated regions (left) or nucleosomes (right); white spaces in the left panel represent regions connecting methylated and unmethylated Cs.

(D) Probability of methylation protection (light gray), nucleosome occupancy inferred from methylation (Methyl model; gray), and nucleosome occupancy measured by MNase assay (black dashed line) on the background *HOpr*.

(E and F) Same as in (C) except for a sequence containing a single WT (E) or mutant (F) Abf1 motif. Gray vertical lines with red asterisk mark the locations of the motif.

(G) NDR length and proportion generated by the WT (top) or mutant (bottom) motifs. Gray, purple, and orange colors represent *tetO* site, strong NDF (group 1) motifs, and weak NDFs (group 2), respectively. The different brightness of each color represents the different position and copy number of corresponding NDF motifs. The black dashed lines represent the NDR length (148 bp) and proportion (30%) predicted from the background sequences.

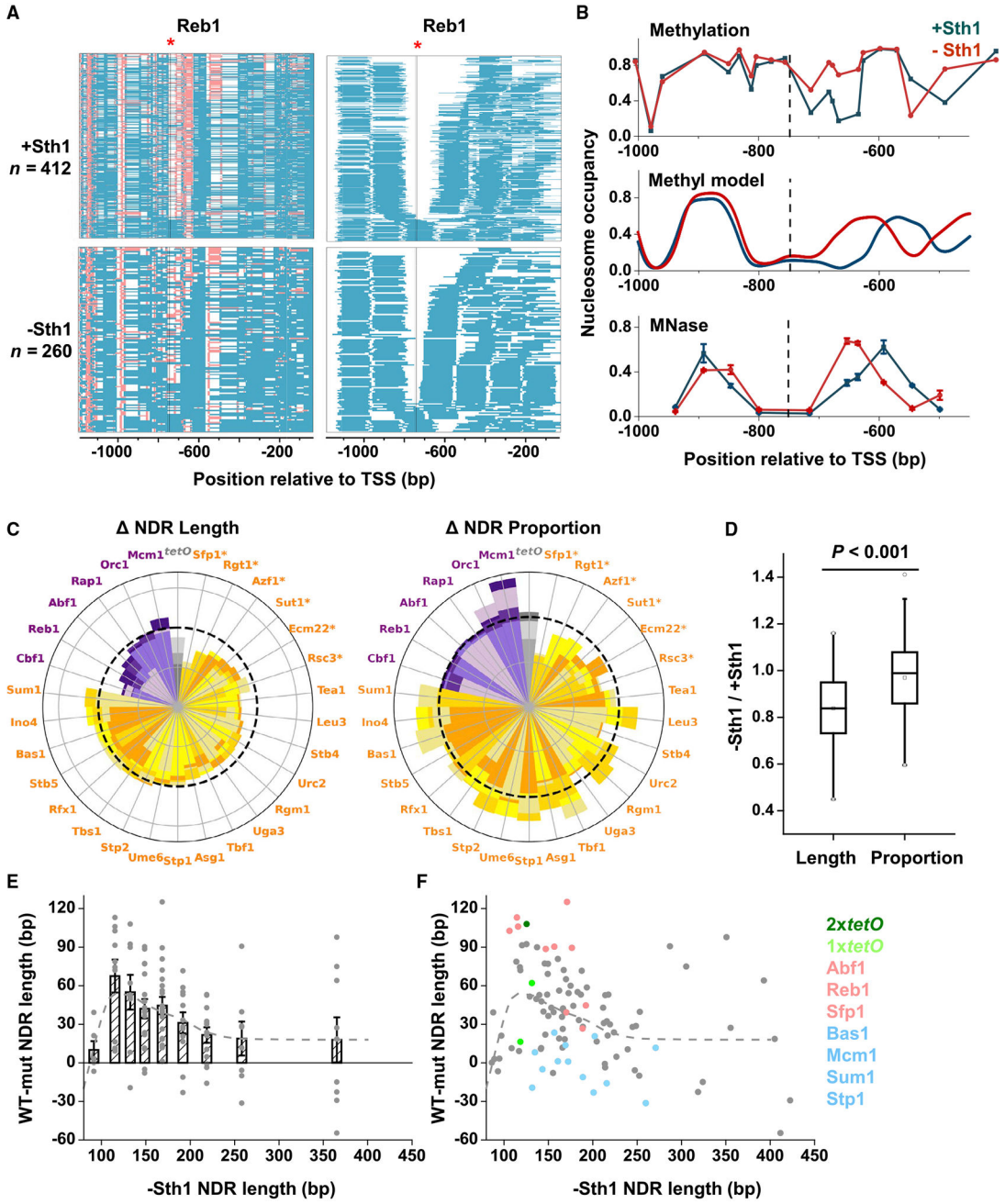

Figure 2. Differential responses to RSC depletion among NDRs

(A) Methylation and inferred nucleosome positioning on a sequence containing a single Reb1 binding site with or without Sth1. Gray vertical line with red asterisk marks the location of the Reb1 motif.

(B) Proportion of methylation protection (top), nucleosome occupancy inferred from methylation (middle), and nucleosome occupancy measured by MNase assay (bottom) for the Reb1-containing sequence with or without Sth1. MNase assay was repeated twice. Error bars represent standard errors.

(C) Effect of Sth1 depletion on NDR length (left) and NDR proportion (right). The −Sth1 to +Sth1 ratios were plotted in the radar plots. NDFs were sorted based on the length change. The value of the dash circle is 1 (no change). NDFs showing significant proportion decreases are labeled with asterisks.

(D) The change on NDR length and proportion caused by Sth1 depletion averaged among 102 NDRs shown in (C). Error bars represent 95% confidence interval.

(E) The change in NDR length (+Sth1 minus −Sth1) versus −Sth1 NDR length. −Sth1 NDR lengths were divided into bins, and average ΔNDR length was calculated for each bin. The smoothed curve (dashed line) represents the average length dependence of the RSC effect. Error bars represent standard errors.

(F) ΔNDR length versus −Sth1 NDR length on individual synthetic sequences is compared with the average length dependence. Some NDFs that are sensitive or insensitive to RSC depletion are colored in pink and blue, respectively. Dark and light green data points represent ISO sequences with two and one *tetO*, respectively.

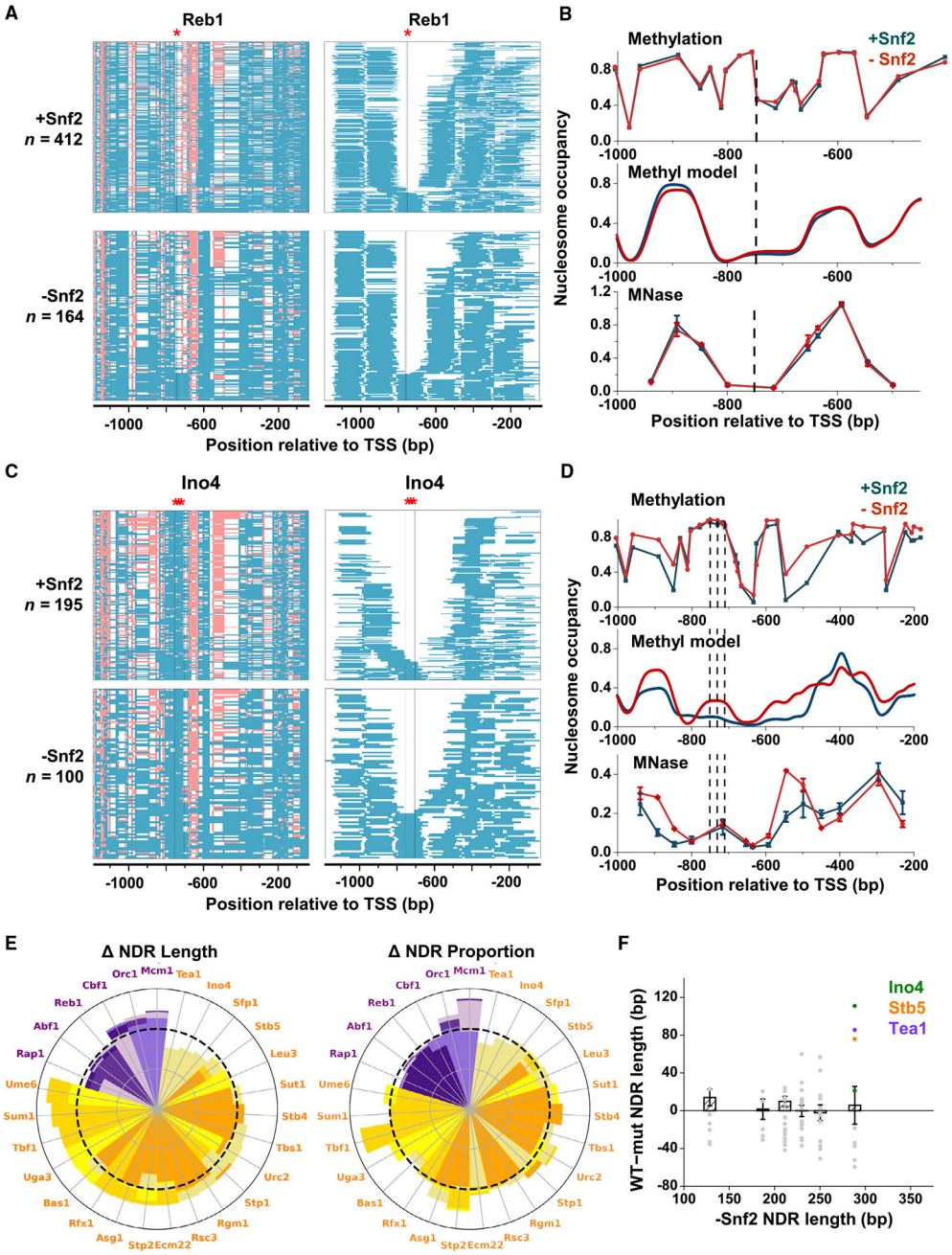

Figure 3. Ino4, Stb5, and Tea1 recruit SWI/SNF to generate extra-long NDRs

(A and B) Nucleosome positioning measured by methylation and MNase on sequences containing one Reb1 motif with or without Snf2. MNase assay was repeated twice. Error bars represent standard errors.

(C and D) Nucleosome positioning measured by methylation and MNase on sequences containing three Ino4 motifs with or without Snf2. MNase assay was repeated twice.

(E) Ratio change of NDR length and proportion upon Snf2 depletion.

(F) The change in NDR length (+Snf2 minus −Snf2) versus −Snf2 NDR length. Lengths of 71 NDRs were divided into bins, and average ΔNDR length was calculated for each bin. Error bars represent standard errors.

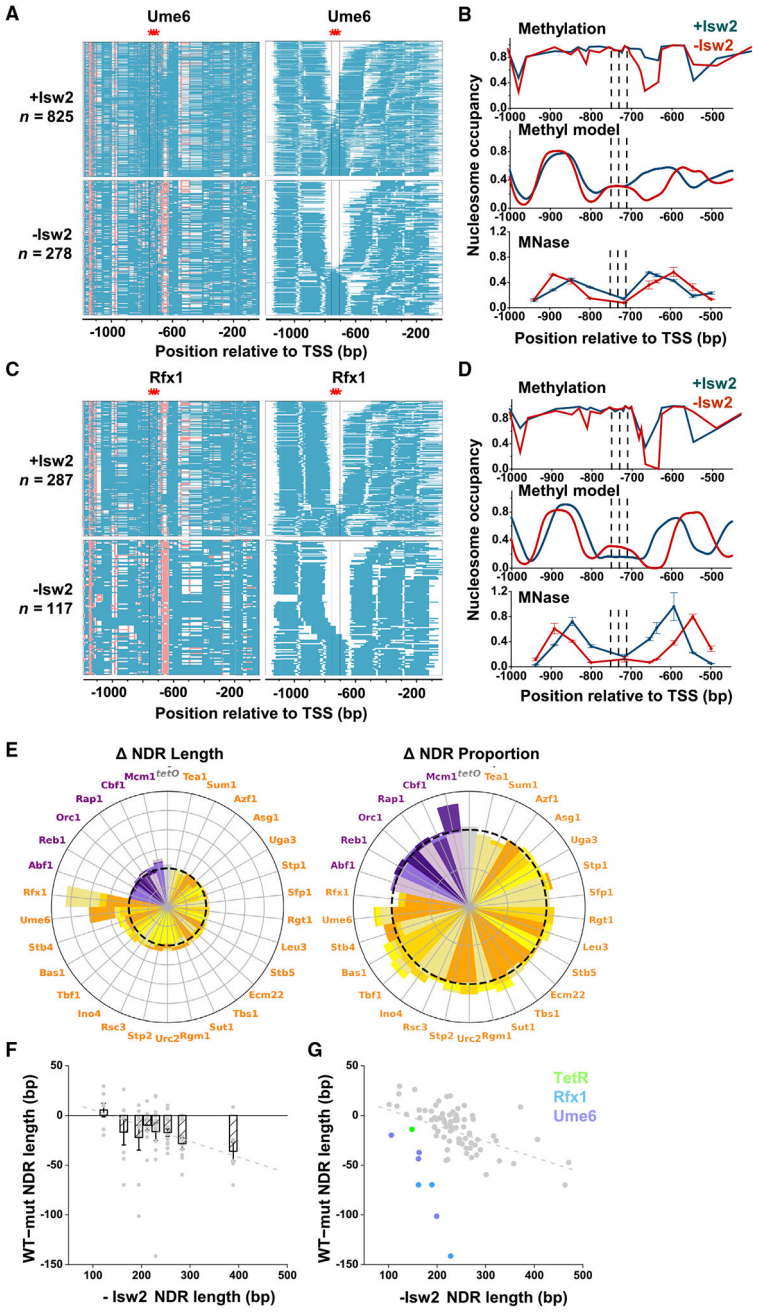

Figure 4. Ume6 and Rfx1 recruit ISW2 to generate extra-short NDRs

(A–D) Nucleosome positioning measured by methylation and MNase on sequences containing Ume6 (A and B) and Rfx1 (C and D) motif with or without Isw2. MNase assay was repeated twice. Error bars represent standard errors.

(E) Ratio change of NDR length and proportion upon Isw2 depletion.

(F) The change in NDR length (+Isw2 minus −Isw2) versus −Isw2 NDR length. Eighty-three NDR lengths were divided into bins, and average ΔNDR length was calculated for each bin. The average length dependence of ISW2 was fitted by a straight line. Error bars represent standard errors.

(G) ΔNDR length versus −Isw2 NDR length on individual synthetic sequences was compared with the average length dependence. NDFs strongly affected by Isw2 depletion (Rfx1 and Ume6) are shown in blue and purple. The green data point represents TetR.

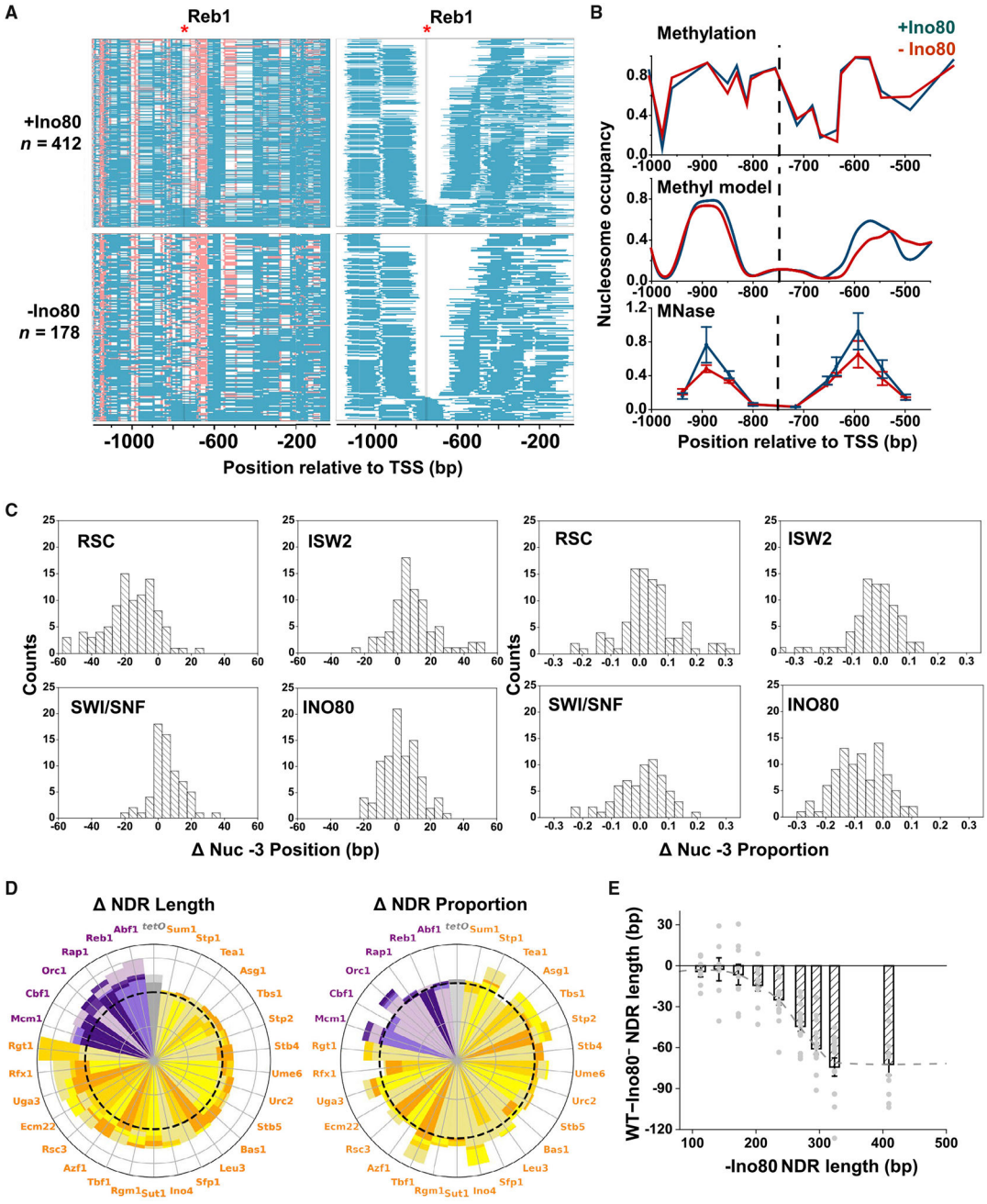

Figure 5. INO80 nonspecifically shrinks most NDRs

(A and B) Nucleosome positioning measured by methylation and MNase on sequences containing a Reb1 motif with or without Ino80. Error bars represent standard errors.

(C) Histograms of the position and occupancy change of nucleosome −3 (the nucleosome immediately downstream of the NDFs) upon the depletion of CRs (−CR minus +CR).

(D) Ratio change of NDR length and proportion upon Ino80 depletion.

(E) The change in NDR length (+Ino80 minus −Ino80) versus −Ino80 NDR length. −Ino80 NDR lengths were divided into bins, and average ΔNDR length was calculated for each bin.

The number of NDRs in the analysis is 103. The smoothed curve (dashed line) represents the average length dependence of the INO80 effect. Error bars represent standard errors.

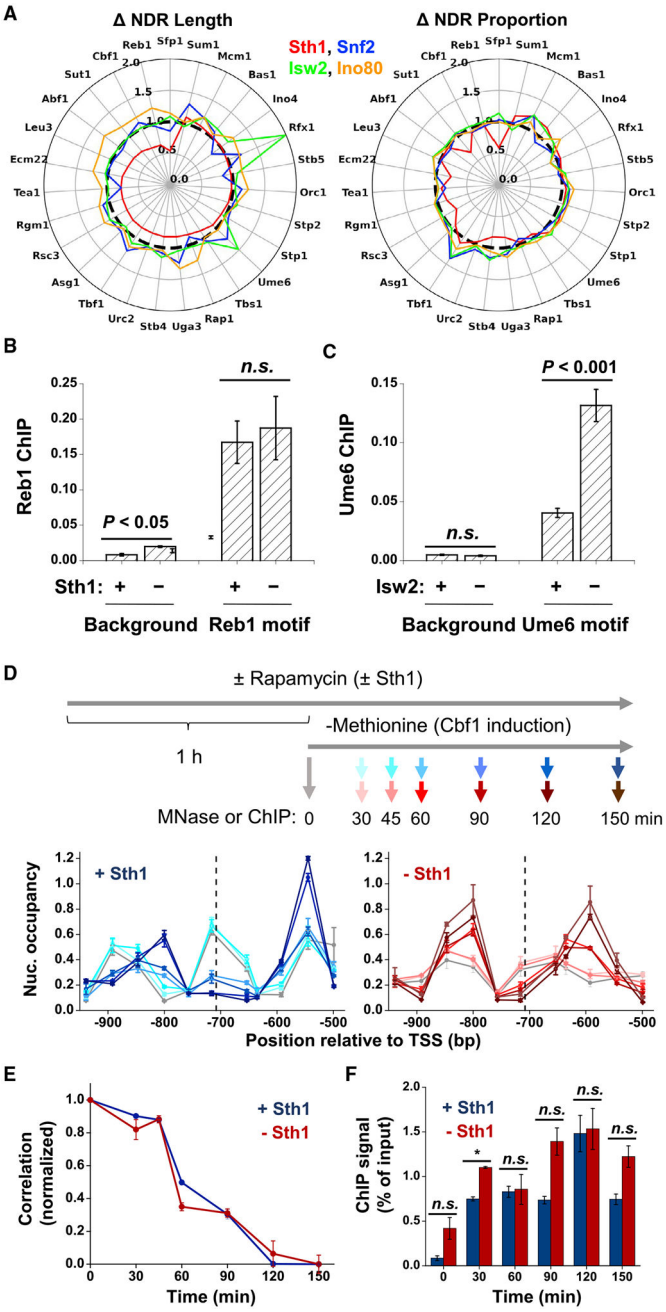

Figure 6. Binding and nucleosome invasion of NDFs do not require CRs

(A) Changes of NDR length and proportion upon the depletion of Sth1, Snf2, Isw2, and Ino80.

(B) Reb1 ChIP-qPCR results on template with or without Reb1 motif ± Sth1. These four conditions have four, two, seven, and six replicates, respectively. Error bars represent standard errors.

(C) Ume6 ChIP-qPCR results on template with or without Ume6 motifs ± Isw2. These four conditions have two, two, six, and six replicates, respectively. Error bars represent standard errors.

(D) MNase measurement of nucleosome occupancy over a sequence containing one Cbf1 binding site (marked by the dashed line) at different time points of Cbf1 induction ± Sth1. Top, the scheme of experiment. Bottom, nucleosome occupancy at different time points; the darker color represents longer Cbf1 induction. Note the decrease of nucleosome occupancy near the Cbf1 binding site over time. Error bars represent standard errors.

(E) Quantification of nucleosome occupancy change in (D). Error bars represent standard errors.

(F) Cbf1 ChIP-qPCR at different time points after Cbf1 induction ± Sth1. Each time point was repeated twice. Student's t test was used to calculate p value. *$p < 0.05$. Error bars represent standard errors.

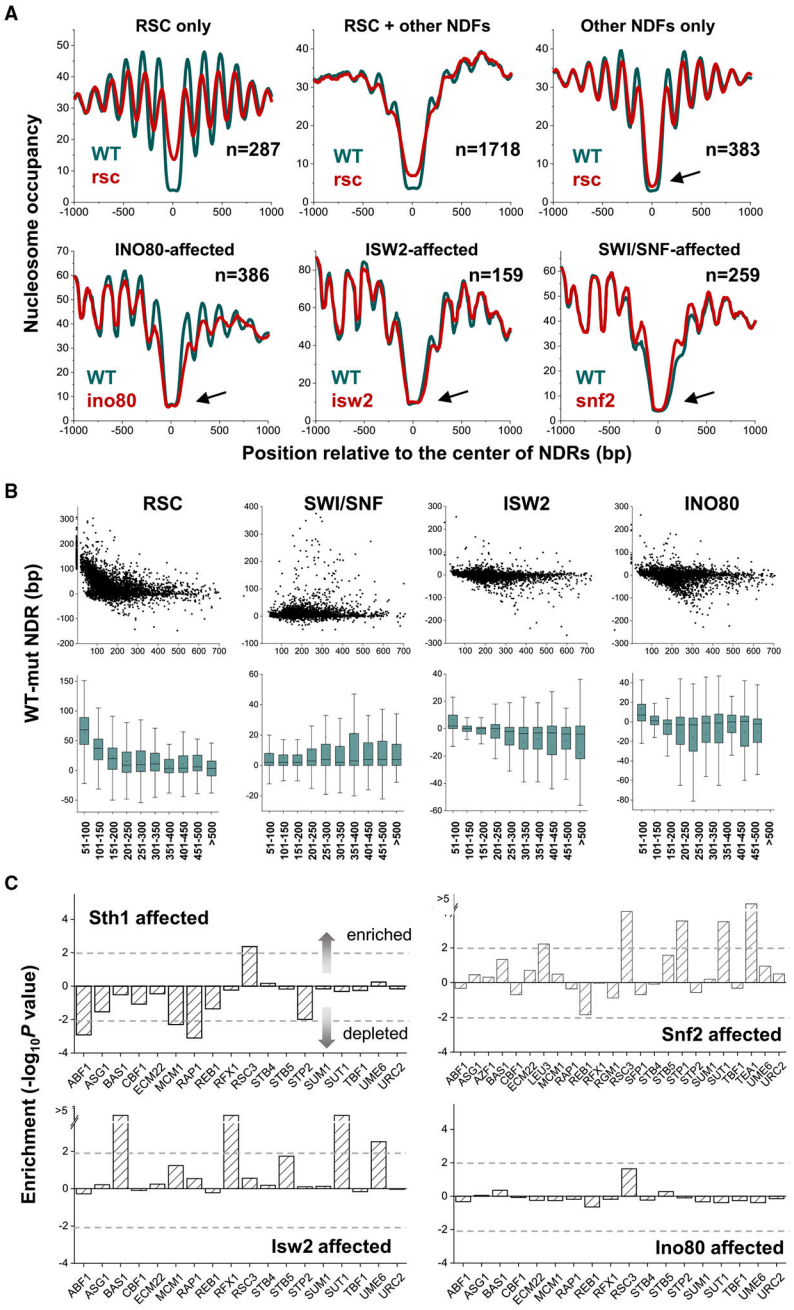

Figure 7. Genome-wide analyses of CR effect support the findings from the ISO library

(A) Average nucleosome occupancy with or without indicated CR near affected NDRs. These plots are aligned at the mid-point of these NDRs. The RSC case is divided based on if the NDR only associates with RSC, or other NDFs, or both.

(B) Change in NDR length (WT – mutant) versus the NDR length in CR-depleted cells. The top plot shows the data for each individual NDR; the bottom is the boxplot for different length bins, where boxes show the 25%–75% data range, and the whiskers represent outliers (1.5 times the interquartile range above and below). Error bars represent 95% confidence interval.

(C) Enrichment of bound NDFs in NDRs that are sensitive to CR depletion in comparison with genome-wide NDRs. The y axes represent $-\log_{10}$ p value, and data points above 2 are considered significant ($p < 0.01$). Data in the positive direction represent factors that are enriched in these NDRs, and the negative ones are depleted.

KEY RESOURCES TABLE

REAGENT or RESOURCE	SOURCE	IDENTIFIER
Antibodies		
anti-TAP antibody	Thermo Fisher	Cat#CAB1001; RRID: AB_10709700
Bacterial and virus strains		
NEB® 5-alpha competent *E. coli*	NEB	Cat#C2987
NEB® 5-alpha Electrocompetent *E. coli*	NEB	Cat#C2989
Chemicals, peptides, and recombinant proteins		
Nuclease micrococcal from *Staphylococcus aureus*	Sigma-Aldrich	Cat#N3755
Protease Inhibitor Cocktail	Sigma-Aldrich	Cat#P8215
Magna ChIP™ Protein A + G Magnetic Beads	Millipore Sigma	Cat#16-663
Proteinase K	Thermo Fisher	Cat#4333793
Z1005 Zymolyase	US Biological	Cat#37340-57-1
IgG Sepharose™ 6 Fast Flow	Cytiva	Cat#17-0969-01
Turbo Cx Pfu	Agilent	Cat#600410
EpiMark® Hot Start Taq DNA Polymerase	NEB	Cat#M0490S
Rapamycin	Life Technologies	Cat#PHZ1235
17β-estradiol	Tocris Bioscience	Cat#50-28-2
Critical commercial assays		
EpiTect Fast DNA Bisulfite kit	Qiagen	Cat#59824
Deposited data		
Analyzed and raw Pacbio sequencing data	GEO database	GEO: GSE199812
Genome-wide MNase-seq data	GEO database	GEO: GSE115412
Genome-wide ChIP-exo data	GEO database	GEO: GSE147927
Experimental models: Organisms/strains		
yHC13-SNF2	This study (Table S4)	N/A
yHC15-bkg	This study (Table S4)	N/A
yHC17	This study (Table S4)	N/A
yHC17-STH1	This study (Table S4)	N/A
yHC28	This study (Table S4)	N/A
yHC28-STH1	This study (Table S4)	N/A
yHC28-INO80-GFP	This study (Table S4)	N/A
yHC28-ISW2-GFP	This study (Table S4)	N/A
yHC49-SNF2	This study (Table S4)	N/A
yHC53-STH1	This study (Table S4)	N/A
yHC53-STH1-Reb1-Reb1	This study (Table S4)	N/A
yHC53-STH1-bkg-Reb1	This study (Table S4)	N/A
yHC53-ISW2-bkg-UME6	This study (Table S4)	N/A
yHC53-ISW2-UME6-UME6	This study (Table S4)	N/A
yHC66-Cbf1	This study (Table S4)	N/A
yCY64-Ume6DBD	This study (Table S4)	N/A

REAGENT or RESOURCE	SOURCE	IDENTIFIER
yCY49-Ume6	This study (Table S4)	N/A
yHC89-5-Reb1	This study (Table S4)	N/A
Oligonucleotides		
MNase-qPCR primers	IDT (Table S4)	N/A
Library construction primers	IDT (Table S4)	N/A
Recombinant DNA		
pCY20	Yan et al., 2018	N/A
pHC03-FRB-TAP	This study	N/A
pHC04-FRB-GFP-TAP	This study	N/A
pHC06	This study	N/A
pHC09-TetR	This study	N/A
pHC11-GC (backbone without oligo)	This study	N/A
pHC11-oligo-GC (backbone with oligo)	This study	N/A
pHC21-FRB-GFP	This study	N/A
pHC23-Cbf1-TAP	This study	N/A
pHC23-REB1-TAP	This study	N/A
pHC23-UME6-TAP	This study	N/A
pAD1161 (full sequence available on request)	This study	N/A
pMJ1314 (full sequence available on request)	This study	N/A
Software and algorithms		
OriginPro	Originlab	N/A
ImageJ	NIH	N/A
MATLAB	Math Works	N/A
computeMatrix	deepTools	N/A
Plotheatmap	deepTools	N/A
Matplotlib	https://matplotlib.org/	N/A